

2021

Characterizing heterotopic ossification development following muscle injury

<https://hdl.handle.net/2144/43435>

"Downloaded from OpenBU. Boston University's institutional repository."

BOSTON UNIVERSITY
SCHOOL OF MEDICINE

Thesis

**CHARACTERIZING HETEROTOPIC OSSIFICATION DEVELOPMENT
FOLLOWING MUSCLE INJURY**

by

ADRIAN R. ILINSKI

B.S., University of Connecticut, 2015

Submitted in partial fulfillment of the
requirements for the degree of
Master of Science

2021

© 2021 by
ADRIAN R. ILINSKI
All rights reserved

Approved by

First Reader

Beth Bragdon, Ph.D.
Assistant Professor of Orthopaedic Surgery

Second Reader

Louis C. Gerstenfeld, Ph.D.
Professor of Orthopaedic Surgery

ACKNOWLEDGMENTS

I would like to thank Dr. Bragdon and Dr. Louis Gerstenfeld for their continuous support and guidance throughout this project. I would also like to thank Anne Hinds, Jack Page and Aaron Nakasone for their assistance.

**CHARACTERIZING HETEROTOPIC OSSIFICATION DEVELOPMENT
FOLLOWING MUSCLE INJURY**

ADRIAN R. ILINSKI

ABSTRACT

Introduction:

Musculoskeletal trauma is a well-known cause of heterotopic ossification, also known as ectopic ossification, a pathological process in which bone forms within soft tissues. Previous studies in the lab have shown that muscle trauma increases the amount of bone formed in demineralized bone matrix-induced animal models. Moreover, recent studies have shown that ectopic ossification's underlying mechanism follows a specific gene expression progression similar to endochondral ossification. Because of the inherent complexity of the biological composition of DBM, the need to use immune deficient animals with human DBM, and the experimental objective to clarify the role of BMP2 in the inductive process on musculoskeletal trauma on ectopic bone formation a simpler and better defined model of inducing ectopic bone formation was examined. For the studies reported here, defined concentrations of BMP2 were added to gelatin sponges in combination with a defined muscle injury to induce ectopic bone formation on bone formation.

Objective:

Characterize the effects muscle trauma on ectopic bone formation using absorbable gelatin sponge/BMP2 – induction model for ectopic bone formation.

Bone volume and structure were assessed by MicroCT. The quantitative expression of specific mRNAs was used to examine: the induction and recruitment of stem cells: skeletal cell development and differentiation; and BMP signaling.

Methods:

Tamoxifen inducible B6.Cg-Pax7^{tm1(cre/ER2)Gaka/J} transgenic mice were crossed with B6.Cg-Gt(ROSA)26Sor^{tm14(CAG-tdTomato)Hze/J} to create Pax7/Ai14 reporter. These animals were subsequently crossed with B6.129S7-Rag1^{tm1Mom/J} mice. This created an inducible reporter mouse capable of receiving the absorbable gelatin sponge loaded with recombinant human bone morphogenic protein 2 (BMP-2). Between 8-10 weeks of age, mice received two tamoxifen injections within 48 hours apart, followed by a washout period of 96 hours. Animals were implanted with 0.2 cm³ of sterile absorbable gelatin sponged loaded with 0.3 µg of BMP-2 along the periosteal surface of the femur bilaterally. Muscle injury was induced in select animals following surgery. Animals were harvested at either postoperative day (POD) two, eight, or sixteen. Tissue samples were either prepared for plain film radiographs and micro-computed tomography (µCT) or mRNA extraction. Samples selected for imaging were radiographed using plain film and then proceeded for µCT. Micro-computed tomography allowed for analysis of the ectopic bone and the creation of 3D renderings. Implant samples selected for mRNA extraction were further prepared to analyze gene expression using real time quantitative polymerase chain reaction (qPCR).

Results:

Muscle trauma did not significantly change the characteristics of ectopic bone formed in the BMP-2 supplemented absorbable gelatin sponge implant.

However, a batch effect had been observed between samples that received two different batches of BMP-2, which differed significantly in tissue volume and trabecular morphology. Gene expression showed a progressive pattern of expression. *Sox2* expression peaked early in POD 2 samples. In comparison, *Prx1* and α -SMA expression peaked later on at POD 8 and 16. Early markers of chondrogenesis, *Sox9*, and *Acan*, peaked at POD 8, while late makers of chondrogenesis, *Col10a1*, and osteogenesis markers, *RUNX2*, *Sp7*, and *DMP-1*, peaked at POD16. Expression of various members of the BMP gene family showed that BMPs were endogenously induced over the course of ectopic bone formation and suggests that BMP signaling is central to progressive development of ectopic bone formation.

Conclusion:

Skeletal muscle injury does not appear to significantly impact the formation of ectopic bone in gelatin sponge implants supplemented with 0.3 μ g of BMP-2. However, batch 2 samples showed some distinction between injured and noninjured samples, but the sample size was too small to make any firm conclusion. Further studies with the same protocol would help create a more definitive conclusion. RNA analysis reaffirmed a previous study's findings showing a progression of gene expression similar to endochondral ossification.

However, this study produced evidence suggesting a delay in either osteogenesis or in the apoptosis and resorption of the hypertrophic cartilage within this model. Further studies could introduce later harvest times at 21 or 31 days postoperative, allowing a better understanding of when osteogenesis peaks during ectopic ossification.

TABLE OF CONTENTS

ACKNOWLEDGMENTS	iv
ABSTRACT	v
TABLE OF CONTENTS	ix
LIST OF TABLES	xi
LIST OF FIGURES	xii
LIST OF ABBREVIATIONS	xiii
INTRODUCTION	1
<i>Endochondral Ossification</i>	2
<i>Heterotopic Ossification</i>	6
<i>Stem Cells</i>	8
<i>Skeletal Muscle & Satellite Cells</i>	9
<i>Role of Muscle In Osteogenesis</i>	11
METHODS.....	14
<i>Materials</i>	14
<i>Animals</i>	14
<i>Tamoxifen Injections</i>	14
<i>Sponge Implant Surgery</i>	15
<i>Harvest & X-ray Imaging</i>	15
<i>Micro-Computed Tomography</i>	16

<i>RNA extraction</i>	17
<i>Gel Electrophoresis and Spectroscopy</i>	18
<i>RNA Purification</i>	19
<i>cDNA Production</i>	20
<i>Quantitative Polymerase Chain Reaction</i>	21
<i>Statistical Analysis</i>	21
RESULTS	23
<i>Evaluating the Effects of Muscle Trauma on Heterotopic Ossification</i>	23
<i>Comparing Gene Expression within the Implant During Ectopic Ossification</i> ..	29
<i>Stem Cell Marker Expression</i>	29
<i>Chondrogenesis Marker Expression</i>	31
<i>Osteogenesis Marker Expression</i>	34
<i>BMP Signaling Expression</i>	34
DISCUSSION	37
<i>Effect of BMP-2 Batch on Ectopic Bone</i>	37
<i>Effects of Muscle Trauma Ectopic Bone Development</i>	37
<i>Variations in Gene Expression in Heterotopic Ossification Over Time</i>	38
<i>Conclusion and Limitations</i>	40
REFERENCES	42
CURRICULUM VITAE	49

LIST OF TABLES

Table	Title	Page
1	qPCR Primers	22

LIST OF FIGURES

Figure	Title	Page
1	Overview of Endochondral Ossification	3
2	Plain Film Radiographs Demonstrating the Effects of Time and BMP-2 Batch Effect on Ectopic Bone Formation	24
3	Effects of Injury on Ectopic Bone	26
4	Effects of BMP-2 Batch on Ectopic Bone	27
5	3D Renderings Demonstrating Effect of BMP-2 Batch on Tissue Mineralization	28
6	Position of Ectopic Bone Along the Femur	29
7	Comparison of Stem Cell Markers in Ectopic Bone Over Time	32
8	Comparison of Chondrogenic Markers in Ectopic Bone Over Time	33
9	Comparison of Osteogenic Markers in Ectopic Bone Over Time	35
10	Comparison of BMP Signaling Markers in Ectopic Bone Over Time	36

LIST OF ABBREVIATIONS

3D	Three-dimensional
Acan	Aggrecan
ACVR1	Activin A type 1 Receptor
α -SMA	alpha smooth muscle actin
BMP	Bone Morphogenetic Protein
BMP-2	Bone morphogenetic protein 2
BMP-7	Bone morphogenetic protein 7
BMPR-1	Bone Morphogenetic Protein Receptor type 1
BMPR-2	Bone Morphogenetic Protein Receptor type 2
BV	Bone volume
CD	Cluster of differentiation
cDNA	complementary DNA
Col10a1	Collagen type 10 alpha 1
Col2a1	Collagen type 2 alpha 1
DMP-1	Dentin matrix acidic phosphoprotein 1
FGF	Fibroblast Growth Factor
FOP	Fibrodysplasia Ossificans Progressiva
HH	Hedgehog
HO	Heterotopic Ossification
Id-1	Inhibitor of DNA binding
IHH	Indian Hedgehog

MSTN	Myostatin
MyoD	Myoblast determination protein 1
NOG	Noggin
NSAID	Non-steroidal anti-inflammatory drug
Pax7	Paired box 7
PBS	Phosphate buffer solution
POD	Postoperative day
Prx1	Paired related homeobox 1
RUNX2	Runt-related Transcription Factor
Sox2	sex determining region Y-box 2
Sox5	Sex Determining Region Y-box 5
Sox6	Sex Determining Region Y-box 6
Sox9	Sex Determining Region Y-box 9
Sp7	Osterix
SRY	Sex Determining Region Y
TbN	Trabecular number
TbSp	Trabecular spacing
TbTh	Trabecular thickness
TV	Tissue volume
VEGF	Vascular Endothelial Growth Factor

INTRODUCTION

Fractures are one of the most frequently seen large-organ injury with around 16 million fractures annually in the United States alone. These fractures will heal to their pre-injury state most of the time; however, approximately 5-10% will result in impaired healing or nonunion (Coates et al., 2019; Einhorn & Gerstenfeld, 2015). Complications like these lead to increased hardship to the patient, including potential disability, decreased quality of life, the increased financial burden with prolonged healthcare management, and prolonged prescription usage (Ekegren et al., 2018). Current treatment options can be categorized as either physical stimulation, which utilizes devices to mechanically stimulate bone formation by applying stress onto the bone tissue, or biological therapies, including autologous growth factors or hormones to promote osteogenic cell differentiation and proliferation. The current gold-standard treatment to enhance bone regeneration is autologous bone grafting, often using the iliac crest due to enrichment of both osteogenic and angiogenic progenitor cells. Despite the excellent results with this procedure, it is costly and frequently associated with pain and other complications such as injury, hematoma, and even fracture at the harvest site (Buza & Einhorn, 2016). These limitations emphasize the need to further understand the biological processes involved in bone formation and fracture healing to find novel treatments that are

less invasive to cater to the high number of patients suffering from impaired fracture healing.

Endochondral Ossification

Bone ossification or osteogenesis is divided into two distinct types, intramembranous and endochondral. Intramembranous ossification utilizes a template of condensed mesenchymal cells that directly differentiate into osteoblasts, which secrete an unmineralized collagen-proteoglycan matrix that later binds calcium hardening and forming bone. This is the predominant process during clavicle development and most of the craniofacial skeleton (Breeland et al., 2020). In contrast, the remainder of the axial skeleton and appendicular skeleton develops through endochondral ossification, which, as shown in Figure 1, uses hyaline cartilage as an intermediate tissue that is gradually replaced with bone (Vortkamp et al., 1998). The progression of bone development through endochondral ossification can be summarized into five stages: the condensation of mesenchymal cells at the site of a future bone, development of a hyaline cartilage model, calcification of cartilage and formation of the bone collar, the formation of the primary ossification center, and the formation of secondary ossification centers (Breeland et al., 2020).

The process of skeletogenesis begins with the migration of mesenchymal stem cells from their embryonic origin to the site of the future bone, where the cells condense into the shape and size that will serve as a model of the future

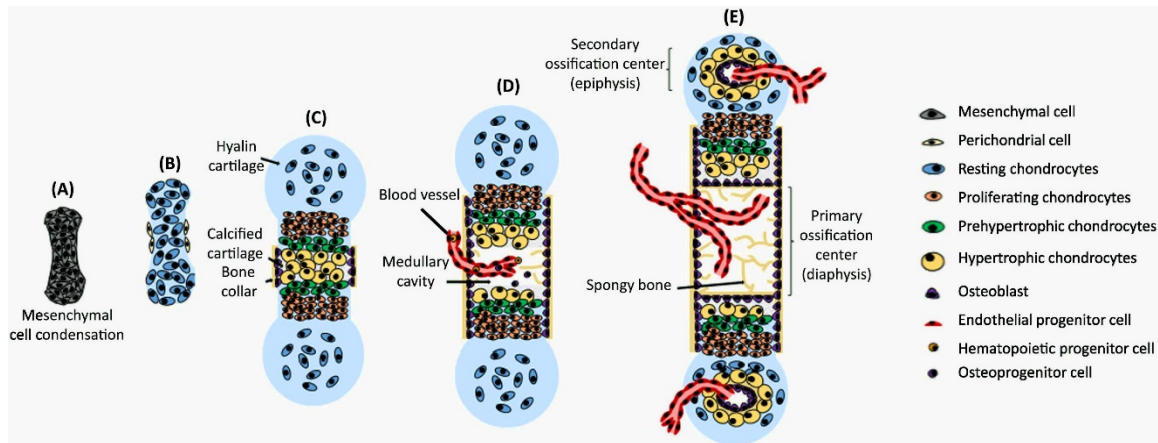


Figure 1: Overview of Endochondral Ossification. Illustrative depiction of endochondral ossification progression through several stages. Modified from (Allas et al., 2019).

bone (Berendsen & Olsen, 2015). This mesenchymal condensation is characterized by a densely packed cluster of cells with increased expression of neural cell adhesion molecules and neural cadherins, which mediate cell-cell adhesions during this phase. Several molecules have been shown to contribute to the aggregation of mesenchymal cells, including Homeobox A 13, Homeobox D 13, bone morphogenetic proteins (BMPs), noggin (NOG), and fibroblast growth factors (FGFs) (Long & Ornitz, 2013).

Transition to the next phase of endochondral ossification is marked by the acquisition of chondrogenic potency by the mesenchymal cells and differentiation into chondrocytes. This commitment to the chondrocyte lineage is regulated by the expression of sex determining region Y (SRY)-box 9 (*Sox9*). *Sox9* further activates two other member *Sox* family transcription factors, SRY-box 5 (*Sox5*) and SRY-box6 (*Sox6*), which cooperate with *Sox9* in chondrocytic differentiation (Akiyama & Lefebvre, 2011; Bi et al., 1999). The *Sox5*, *Sox6*, and *Sox9* form a

trio of transcription factors that are essential for the expression of several chondrocyte-specific genes including, collagen type 2 alpha 1 (*Col2a1*) and aggrecan (*Acan*), genes that encode for the dominant fibrous and ground substance components of hyaline cartilage (de Crombrugge et al., 2000; Han & Lefebvre, 2008). Simultaneously, Sox5, Sox6, and Sox9 stimulate the rapid proliferation of chondrocytes leading to linear growth (Allas et al., 2019). In addition to stimulating proliferation, previous research has identified Sox9 expression in chondrocytes as a vital regulator of endochondral ossification progression through hypertrophy inhibition (Akiyama et al., 2002; Bi et al., 2001). Conversely, the expression of Runt-related transcription factor 2 (*RUNX2*) initiates as chondrocytes begin to hypertrophy and is maintained throughout the hypertrophic cell's life. Expression of *RUNX2* facilitates the transcription of collagen type 10 alpha 1 (*Col10a1*), metalloproteinase 13, and vascular endothelial growth factor (*VEGF*), factors that facilitate the remodeling of the cartilage matrix and infiltration of blood vessels essential for osteogenesis (Hata et al., 2017; Hattori et al., 2010).

The expression of *RUNX2* primarily regulates the commitment to the osteogenic lineage and is upstream of osterix (*Sp7*). Previous studies demonstrated mutant mice lacking either *RUNX2* or *Sp7* failed to produce osteoblasts (Komori et al., 1997; Nakashima et al., 2002). In turn, *RUNX2* and *Sp7* regulate the expression of alkaline phosphatase, secreted phosphoprotein 1, and bone gla protein, essential osteoblast-specific genes (Ohba, 2020). Several

extracellular factors have been shown to regulate the expression of *RUNX2* and *Sp7*, including Indian hedgehog (IHH), NOG, Wnts, BMPs, and FGFs, and by doing so, regulating the differentiation of osteoblasts (Long & Ornitz, 2013). Of these, BMPs are one of the best-understood regulators of osteogenesis. It is currently understood that the binding of BMPs to both bone morphogenetic protein receptor type 1 (BMPR-1) and type 2 (BMPR-2) permits the phosphorylation of BMPR-1 by BMPR-2, which is constitutively active, activating the type 1 receptor kinases. In turn, BMPR-1 kinases phosphorylate Smad1, Smad5, or Smad8, which will form a complex with Smad4 and bind to DNA, upregulating the expression of osteogenic genes like *RUNX2* and *Sp7* as well as upregulating inhibitor of DNA binding 1 (*Id-1*), which inhibits myogenesis (B. Bragdon et al., 2011; Katagiri et al., 2015).

Early sources of osteogenic precursors contributing to endochondral ossification are the diaphyseal perichondrium adjacent to pre-hypertrophic and hypertrophic chondrocytes. As opposed to intramembranous ossification, the secretion of IHH by these hypertrophic cells is vital in inducing *RUNX2* and *Sp7* expression in perichondrial osteogenic progenitor cells during endochondral ossification and leading to the formation of the bone collar (St-Jacques et al., 1999). Following the bone collar development, osteogenic progenitor cells infiltrate the diaphysis via blood vessels formed due to *VEGF* expression by hypertrophic chondrocytes. These osteogenic progenitor cells differentiate into osteoblasts and form the primary ossification center. These steps will then be

repeated at each epiphysis and form the secondary ossification centers (Hallett et al., 2019).

Heterotopic Ossification

Heterotopic ossification (HO), also referred to as ectopic ossification, is the abnormal deposition of bone within soft tissue, like skeletal muscle, tendons, ligaments, and nervous tissue (Barfield et al., 2017). HO is divided into two forms, trauma-induced and the much rarer genetic form. One of the most debilitating genetic HO is fibrodysplasia ossificans progressiva (FOP). FOP is characterized by episodic inflammation of the soft tissues, which results in the formation of bone replacing skeletal muscle and connective tissues leading to the progressive immobility of joints (Kaplan et al., 2013). Causes of FOP have been linked to a dysregulation of the BMP pathway, and in particular, one study identified the activin A type 1 receptor (*ACVR1*), a *BMPR-1*, gene as a common mutation in both familial and sporadic cases of FOP (Shore et al., 2006). This mutation results in the destabilization of the receptor's glycine-serine activation domain, leading to a loss of its autoinhibition, leading to the expression of downstream osteogenic genes (Kaplan et al., 2013).

Acquired HO can occur following several types of tissue trauma, including fractures, orthopedic surgeries, burns, amputations, and blast injuries. The incidence of HO in the population has a high degree of variability depending on the trauma. Fractures and dislocation have shown to have an incidence of 30%,

while spinal cord injuries and severe amputations have shown occurrences upwards of 50% and 90%, respectively (Meyers et al., 2019). The mechanisms that drive acquired HO are not yet fully understood. The BMP signaling pathway is a critical participant in upregulating osteogenic gene expressions like *RUNX2* and *Sp7*. However, several other pathways may play a role in regulating osteoblast differentiation via an independent mechanism or BMP crosstalk; these include the transforming growth factor beta, pathogen-associated molecular patterns, and damage-associated molecular patterns, Wnt/beta-catenin, hedgehog (HH), and mechanistic target of rapamycin kinase pathways (C. Kan et al., 2018; Pulik et al., 2020).

One of the biggest concerns currently with HO is the lack of viable non-operative management. Current methods focus on preventative care using non-steroid anti-inflammatory drugs (NSAIDs), radiotherapy, and bisphosphates. The effectiveness of bisphosphates has been put into question, and though NSAIDs and radiotherapy have shown to decrease HO incidence, there are significant risks, particularly as prophylaxis following fracture surgery. However, once an individual develops HO, minimal that can be done non-operatively, and symptomatic patients likely proceed to excisional surgery (Eisenstein et al., 2018).

Current studies into HO have utilized animal models to study the underlying mechanisms and discover more efficient and effective treatments of this pathological process. Animal models are typically divided into those

designed to mimic the hereditary form of HO and those that replicate the acquired form. The most common genetic models use animals with mutations to the ACVR1 resulting in constitutive activation and upregulation of downstream osteogenic genes, leading to ectopic ossification through an FOP-like mechanism. Conversely, several acquired HO models are currently used, of which BMP injection/implantation is one of the most commonly used due to its simplicity and reproducibility (Cappato et al., 2020; L. Kan & Kessler, 2011). Though these models provide a good representation of heterotopic ossification, its application clinically is limited by its failure in addressing one of the most common causes of HO in humans, trauma. Liu et al. developed a model to address this issue by injecting mice quadriceps with hydrogel and bone morphogenetic protein 2 (BMP-2) and inducing trauma. Their study found that 1 μg of BMP-2 combined with muscle trauma significantly increased bone mineralization compared to animals that only received 1 μg BMP-2 injections. This model provided a better representation of post-traumatic HO and a new model to study the pathological process mechanisms (Liu et al., 2014).

Stem Cells

Stem cells are a type of cell that maintains self-renew capability and potency to differentiate into a more specialized cell. The potency of a stem cell refers to its ability to differentiate into different cell lineages. Stem cells are classified by their potency and are as follows: totipotent, pluripotent, multipotent,

and unipotent. A stem cell that can differentiate into every cell type, including that of the placenta and other extraembryonic tissues, is termed a totipotent stem cell. On the other hand, pluripotent stem cells can differentiate into every cell type originating from the three primary germ layers. Once a stem cell can only differentiate into a cell line of a specific germ layer, it is referred to as a multipotent stem cell (B. C. Bragdon & Bahney, 2018). Several stem cells continue to exist in the adult body referred to as adult stem cells or somatic stem cells. These cells function to regenerate specific tissues postnatally and exist in niches throughout the body, including the blood, intestine, skin, hair follicle, and bone (Matsushita et al., 2020).

The process of fracture healing and heterotopic ossification rely on multipotent stem cells' presence and ability to differentiate into osteoblasts. The periosteum, endosteum, and bone marrow have been known to contain osteogenic progenitor cells contributing to fracture healing. However, recently it has been speculated that satellite cells from skeletal muscle and pericytes from vessel walls contribute to the overall process (B. C. Bragdon & Bahney, 2018).

Skeletal Muscle & Satellite Cells

Skeletal muscle is one of the three types of muscle found in the body. It performs various functions, from the more commonly known locomotion and posture maintenance to the secondary roles in metabolic regulation of amino acids and glucose (Frontera & Ochala, 2015). Structurally, skeletal muscle is a

highly organized tissue composed of myofibers at its basic cellular level. Each myofiber is composed of many myofibrils, which run the entire length of the myofiber. Myofibers themselves arrange as a bundle of fibers forming a fascicle, which further organize with other fascicles to form the complete muscle tissue (Mukund & Subramaniam, 2020).

Like bone, skeletal muscle has a degree of regenerative capability, dependent on the niche of adult stem cells located between the sarcolemma and basal lamina of muscle fibers called satellite cells. These cells, characterized by their expression of paired box 7 (*Pax7*), are predominantly quiescent and remain within their niche until activation following an injury to the surrounding muscle tissue (Chen & Shan, 2019). Muscle regeneration is divided into three phases: 1) the inflammatory phase, 2) the satellite cell activation and differentiation phase, and 3) the maturation and remodeling phase.

Upon muscle injury, muscle tissue begins to degenerate, leading to necrosis of the tissue. This pathological change induces an inflammatory response and the recruitment of circulating leukocytes, including neutrophils and two different populations of macrophages, differentiated by their surface markers cluster of differentiation (CD)68⁺/CD163⁻ and CD68⁻/CD163⁺. The CD68⁺/CD163⁻ macrophages secrete pro-inflammatory cytokines interleukin -1 and tumor necrosis factor-alpha, while the CD68⁻/CD163⁺ population of macrophages secretes anti-inflammatory cytokine, interleukin-10, which has shown to induce

satellite cell proliferation and differentiation (Arnold et al., 2007; Schmidt et al., 2019; Yin et al., 2013).

Activation of satellite cells is regulated by several factors, including Wnt, Notch, and sphingolipid signaling. Interestingly, the population of satellite cells involved in regeneration is not localized to the site of injury. Rather satellite cells along the entire myofiber as well as from adjacent fibers and muscles migrate to the site of injury. Once activated, satellite cells will begin to express either myogenic factor 5 or myoblast determination protein 1 (*MyoD*), which controls the process the cell progresses down; Myogenic factor 5 leads to enhanced proliferation *MyoD* leading to myogenic differentiation. Increased levels of *MyoD* in the cell will upregulate downstream myogenic targets, myogenin, myogenic factor 6, and myocyte enhancer factor-2 leading to differentiation into myoblasts. These myogenic cells will fuse with the damaged myofiber, leading to the formation of a nascent muscle fiber indistinguishable from uninjured fibers (Yin et al., 2013).

Role of Muscle In Osteogenesis

It has long been understood that surrounding muscle has a pro-osteogenic effect on fracture healing, with studies having shown that covering fractures with a flap of muscle tissue has increased bone density and union strength (Harry et al., 2008; Richards et al., 1991). The role that muscle tissue plays during fracture healing is multi-modal, with evidence suggesting it plays a role in providing a

vascular supply to bone ends, a source of osteoprogenitor cells, a source of cytokine and other extracellular factors, and lastly, an anti-microbial environment (Chan et al., 2012). More recently, muscle injury has shown to stimulate ectopic osteogenesis within HO animal models injected with BMP-2 via increased production of bone morphogenetic protein 7 (BMP-7), creating an osteoinductive microenvironment, further supporting the idea that muscle injury plays a role in the formation of bone. Several progenitor cell populations have been identified within muscle tissue that has osteoblastic potential. Of these, satellite cells have been shown to differentiate into the chondrocyte lineage and contribute to the fracture callus endogenously though the contribution was minimal compared to contribution following transplantation (Abou-Khalil et al., 2015). Interestingly, later studies indicated that satellite cells rarely differentiate into osteoblasts (Matthews et al., 2016).

However, previous studies performed in the lab used Pax7/Ai14/Rag inducible reporter mice to lineage trace Pax7-positive cells following muscle injury in a BMP-2 implantation mouse model using DBM. These experiments showed the appearance of Pax7-positive cells within ectopic bone formed following muscle injury, suggesting that muscle trauma stimulates the recruitment of satellite cells and contributes to osteogenesis (W. T. Moore, 2019). Despite this, the underlying signaling pathways and the genes involved are not yet fully understood. Therefore, this study aims to clarify the various genes involved in forming ectopic bone following muscular trauma.

SPECIFIC AIMS

Aim 1: Compare the development of ectopic bone with and without muscle injury. Use X-ray imaging, micro-computed tomography, and quantitative real-time polymerase chain reaction to evaluate ectopic bone development differences over time.

Aim 2: Determine the impact muscle trauma to surrounding skeletal muscle has on ectopic bone formation in mice with periosteal BMP-2 loaded gelatin sponges. Use of micro-computed tomography to quantify the volume of periosteal bone mineralization and morphology of the ectopic bone.

METHODS

Materials

Unless stated otherwise, materials and equipment used were supplied by Thermo Fischer Scientific (Waltham, MA).

Animals

All animal studies were approved by the Institutional Animal Care and Use Committee at Boston University. Mice used in studies were housed under standard conditions at the Boston University Animal Facilities. Mouse strain Pax7cre/Ai14/Ragtm1 was bred in-house for use in these studies as previously described (W. T. Moore, 2019). Both female and male mice were used. All mice used were 8-10 weeks of age at the time of surgery. Before beginning any experimentation, mice were evenly assigned to either receive muscle trauma or not immediately following surgery and were further distributed for harvesting at postoperative days 2 (n = 10), 8 (n = 11), and 16 (n = 24).

Tamoxifen Injections

Tamoxifen solution was prepared at a 10 mg/mL concentration by adding 400 mg of tamoxifen powder (Sigma-Aldrich®, St. Louis, MO) to 40 mL of corn oil. Complete solvation of the tamoxifen was achieved through multiple rounds of sonicated ice-cold ethanol baths until the tamoxifen powder was no longer visible. The dissolved tamoxifen solution was then filtered sterilely using a 10-mL

syringe and an in-line 0.45 µm sterile filter. The solution was then aliquoted into 2 mL tubes and stored at -80 °C.

Mice received two tamoxifen injections intraperitoneally, 48 hours apart, at a dose of 10 µL/g of body weight. Surgery was then performed after a washout period of 96 hours.

Sponge Implant Surgery

Mice were anesthetized using a 4% isoflurane in 100% oxygen mix in an anesthesia chamber. Once animals were anesthetized, the mice were transferred to a heated operating field, and a nose cone delivering 2% isoflurane was used to maintain anesthesia. Prior to incision, mice received subcutaneous injections of 0.01 mL of 2.27% Baytril, an antibiotic, and 0.1 mL of Buprenex, an analgesic. Surgical sites were shaved using electric clippers and prepped with Betadine. An incision was created at the lateral hindleg of each limb, providing access to the femur. Before implantation, a Surgifoam® absorbable gelatin sponge was loaded with 0.3 µg of BMP-2. The loaded sponge was implanted in each hind limb against the femoral periosteum. Following implantation and closure of the incision, muscle trauma was induced to assigned animals by dropping a blunt mass from a height of 31 mm (Grode et al., 2017).

Harvest & X-ray Imaging

Mice were harvested at either postoperative days (POD) 2, 8, or 16. Euthanasia was carbon dioxide inhalation followed by cervical dislocation. Limbs intended for mRNA extraction had the femur, implant, and muscle separated and individually placed into a sterile 2 mL microcentrifuge tube and snap-frozen in liquid nitrogen and stored at -80 °C until extraction.

Samples used for x-ray imaging and micro-computed tomography were collected and fixed in 4% paraformaldehyde (Sigma-Aldrich®, St. Louis, MO) at 4 °C for 72 to 96 hours and then washed three times with 1X phosphate buffer solution (PBS). X-ray imaging was performed using the Faxitron MX-20 Specimen Radiography System (Tuscon, AZ), at a setting of 30 kV for 40 seconds, with Denville Scientific HyBlot CL film (Metuchen, NJ) and then stored in 1X PBS at 4 °C until needed for analysis. Films were developed using a Konica Minolta SRX-101A film processor (Wayne, NJ).

Micro-Computed Tomography

Micro-computed tomography (μ CT) was performed only on POD 16 samples, as previous studies in this lab found the earliest time point for mineralization was postoperative day 12, which was consistent with x-ray imaging of POD 8 samples (B. Bragdon et al., 2017). Micro-computed tomography was performed using the SCANCO Medical μ CT 40 Scanner (SCANCO USA Inc., Wayne, PA). Samples were placed in a 20.5 mm tube and scanned at 70 kVp, 114 μ A, a medium resolution, and an integration time of 200

ms. Images were manually contoured around the ectopic bone, and analysis of the ectopic bone volume (BV) was calculated using the SCANCO Medical program at a threshold of 222 as was measured in a previous study performed in the lab (W. T. Moore, 2019). Three-dimensional (3D) renderings were created using the Microsoft® Paint 3D.

RNA extraction

Chemical extraction was used to isolate mRNA from the implant. Tissue samples were placed in 2 mL Eppendorf tubes with 750 μ L of QIAzol® Lysis Reagent (Qiagen® 79306). Samples emersed in the lysing reagent were frozen for at least 10 seconds in liquid nitrogen. A 5 mm stainless steel bead (Qiagen®) was added to each tube before being placed in cassettes (Qiagen®) and lysed using the Qiagen® Tissue Lyser II at 30 Hz. Samples were checked every 2 minutes, and care was taken to refreeze thawed samples if tissue was not completely lysed. Once lysis was complete, samples were moved to another 2 mL tube containing 1 mL of QIAzol® Reagent (Qiagen® 79306) and placed on ice for at least two minutes.

Samples were then treated with 200 μ L of chloroform (Sigma-Aldrich®), vortexed, and set on ice for another 2 minutes. These samples were vortexed again before being centrifuged for 15 minutes at 1400 rpm and 4°C. The aqueous phase of each tube was carefully transferred to a new tube, and an equal amount of isopropanol was added. Tubes were then inverted several

before centrifuging for 30 minutes at 1400 rpm and 4 °C. After 30 minutes, the supernatant was poured out carefully to avoid losing the pellet containing the RNA. The pellet was then washed twice, with 500 μ L of 70% ethanol (Sigma-Aldrich®), and then centrifuged for 5 minutes at 1400 rpm and 4 °C. Following the final wash, the tube was inverted and placed on a Kimwipe to dry. After drying, the pellet was resuspended in RNase-free water. Femur and muscle samples were resuspended in 50 μ L of RNase-free water, while implants were resuspended in 30 μ L. Extracted mRNA samples were stored at -80 °C.

Gel Electrophoresis and Spectroscopy

The quality and concentration of the extracted RNA were analyzed using gel electrophoresis and spectrophotometry. Gel electrophoresis was performed using a 1.5% agarose gel, made with UltraPure™ agarose from Invitrogen and GelStar™ Nucleic Acid Gel Stain from Lonza Group. Loading samples were prepared by combining 7 μ L of water, 2 μ L of 6XAgarose Gel Loading Dye, and 1 μ L of the extracted RNA. The gel was run at 100 V for approximately 90 minutes. Gels were then placed under ultraviolet light to observe bands indicating the presence of nucleic acids.

Spectrophotometry was used to quantify the concentration and the purity of the RNA. A tray containing 16 cuvettes was loaded with 2 μ L of RNA sample with at least two cuvettes filled with RNase-free water as a control. The loaded tray was placed in the NanoDrop-1000 Spectrophotometer, and sample

concentrations (ng/ μ L) and purity ratios (260 nm/280 nm) were measured.

Sample concentrations above 100 ng/ μ L were large enough for complementary DNA (cDNA) production. Samples above 2000 ng/ μ L required further dilution with RNase-free water, and spectrophotometry was repeated. Purity ratios above 1.7 were deemed acceptable for cDNA production. RNA samples with ratios below 1.7 were purified.

RNA Purification

Samples were prepared for purification by combining 15 μ L of the extracted RNA sample with 1.5 μ L of 5M sodium chloride solution and 20.7 μ L of 100% ethanol. Each sample was then pipetted onto a filter cartridge placed inside a collection tube. The collection tube containing the filter cartridge was then centrifuged for 15 seconds at 10,000 rpm. The flow-through in the collection tube was discarded, and 700 μ L of miRNA Wash Solution 1 was pipetted onto the filter cartridge and centrifuged for 10 seconds at 10,000 rpm. Flow-through was discarded, and 500 μ L of Wash Solution 2/3 was added to the filter cartridge and centrifuged for 10 seconds at 10,000 rpm. Flow-through was discarded, and a final wash was performed using another 500 μ L of Wash Solution 2/3 and centrifuged for another 10 seconds at 10,000 rpm. Flow-through was discarded, and the collection tube containing the sample was centrifuged for 1 minute to remove any residual fluid from the filter. The filter cartridge was then removed and placed into a new collection tube, and 50 μ L of RNase-free water was added

to the filter cartilage and centrifuged for 30 seconds at 14,000 rpm. The elute from this final spin contained the purified RNA. The quality and purity of the purified RNA was again tested before being stored at -80 °C.

cDNA Production

A volume containing 1 µg of RNA from each sample was added into a 0.2 mL PCR tube. RNase-free water was added at varying amounts to bring the final total of each tube to 10.4 µL. Reagents and enzymes from the Tawman Reverse Transcriptase Kit were added into a 2 mL Eppendorf tube to create a master mix containing the following volume of reagents per sample, 6.61 µL of MgCl₂, 6.0 µL of dNTP Mix, 3.0 µL of 10X RT Buffer, 1.5 µL of Random Hexamers. After combining the reagents, the mixture was vortexed to homogenize the solution. After vortexing, the enzymes RNase Inhibitor and Taqman Reverse Transcriptase were added to the master mix at a ratio of 0.6 µL and 1.89 µL per sample, respectively, and mixed by pulsating or gently flicking the tube. From the master mix, 19.6 µL was added to each of the previous PCR tubes containing the RNA sample.

Samples were then loaded into an Eppendorf Mastercycler® Personal thermal cycler and underwent a polymerase chain reaction at the following settings: 25 °C for 10 minutes, 37 °C for 60 minutes, 95 °C for 5 minutes, and finally, a 4 °C hold. The resulting cDNA was then diluted with RNase-free water to a ratio of 1:50.

Quantitative Polymerase Chain Reaction

Quantitative polymerase chain reaction (qPCR) was performed using the diluted cDNA for each sample. A master mix was created containing TaqMan® Universal PCR Master Mix from Applied Biosystems® and TaqMan® Gene Expression Assay from Applied Biosystems® at a ratio of 10 µL and 1 µL per sample, respectively. A list of primers used in this study can be found in Table 1. A 96-well qPCR plate was then filled with 11 µL of the master mix and 9µL of the diluted cDNA. Each sample was run in doublet. As a control, 9 µL of RNase-free water and 11 µL of the master mix was also run as a doublet.

Additionally, bone and muscle samples from non-operated Pax7cre/Ai14/Ragtm1 were used to normalize the cycle threshold (Ct) values. The plate was then covered with a Microamp™ optical adhesion film and then centrifuged to remove any air bubbles at 1500 rpm for 2 minutes. Analysis of the plate was done using the AVI 7700 Sequence Detector® from Applied Biosystems®. The qPCR proceeded in the following steps: 50 °C for 2 minutes, 95 °C for 10 minutes, 40 cycles at 95 °C, each lasting 15 seconds, and 60 °C.

Statistical Analysis

Statistical analysis was performed using JMP® Pro 15.2.0. Analyses included multiple Student t-tests when comparing two groups, and one and two-way analysis of variance (ANOVA) followed by the Tukey multiple comparison

tests were performed when comparing three or more groups, with significance being $p < 0.05$. Charts and graphs were created using Microsoft® 365 Excel.

Primer	Catalog Number
Normalization Primer	
<i>18s</i>	Mm04277571_s1
Stem Cell Primers	
<i>Prrx1</i>	Mm00440932_m1
<i>Pax7</i>	Mm01354484_m1
<i>Sox2</i>	Mm03053810_s1
<i>α-SMA (Acta2)</i>	Mm00725412_s1
Chondrogenic Primers	
<i>Sox9</i>	Mm00448840_m1
<i>Acan</i>	Mm00545794_m1
<i>Col10a1</i>	Mm00487041_m1
Osteogenic Primers	
<i>RUNx2</i>	Mm00501584_m1
<i>Sp7 (Osterix)</i>	Mm04933803_m1
<i>DMP-1</i>	Mm00803833_g1
<i>BMP-2</i>	Mm01340178_m1
<i>BMP-7</i>	Mm00432102_m1
<i>Id-1</i>	Mm00775963_g1
Muscle Associated Primers	
<i>MSTN</i>	Mm01254559_m1

Table 1: qPCR Primers.
Primers and corresponding catalog numbers.

RESULTS

Evaluating the Effects of Muscle Trauma on Heterotopic Ossification

Previous work in the lab showed that blunt force trauma can increase the bone volume induced by DBM implantation (W. T. Moore, 2019). However, it is unclear if muscle trauma can enhance ectopic bone formation using other ectopic bone formation models. Therefore, ectopic bone was induced using a different model, implantation of a gelatin sponge loaded with 0.3 μg of BMP-2. Animals received muscle trauma and were compared to control animals which did not receive the muscle trauma. Tissue was harvested at POD 2, 8, and 16. Plain film radiographs were collected to visualize the ectopic bone (Figure 2). Ectopic bone was not detected at POD 2 and 8; however mineralized ectopic bone tissue was detected at POD 16. It should be noted that there appeared to be a batch effect due to BMP-2. The first cohort of animals (n=16) enrolled for the study received previously reconstituted BMP-2 solution, while the remaining animals (n=29) received newly reconstituted BMP-2 solution. The radiographs clearly suggest varying amounts of mineralized ectopic bone tissue between batch 1 and batch 2 of BMP-2. Batch 1 was used to collect BV measurements, while batch 2 was used for BV measurements and gene analysis.

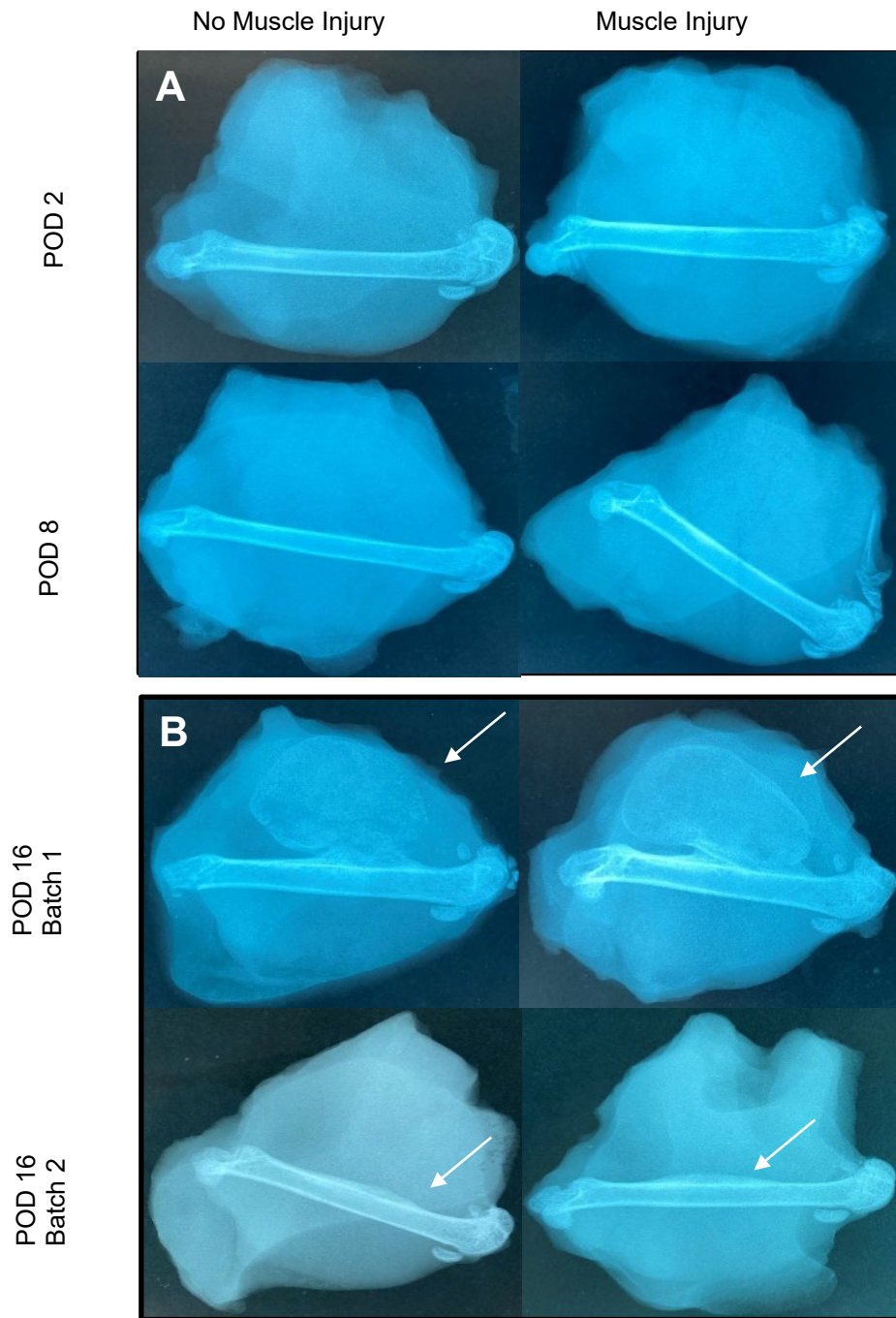


Figure 2: Plain Film Radiographs Demonstrating the Effects of Time and BMP-2 Batch Effect on Ectopic Bone Formation. Above are plain film radiographs of the femur and mineralized ectopic bone tissue of both injured and non-injured mice. A) Samples harvested at POD 2 and POD 8. Both time points show a lack of mineralized ectopic bone tissue. B) Samples harvested at POD 16 contain the first batch and second batch of BMP-2. White arrows indicate where ectopic bone has formed.

Micro-computed tomography was then used to quantify the ectopic bone volume (BV), tissue volume (TV), trabecular number (TbN), trabecular thickness (TbTh), and trabecular spacing (TbSp) at POD 16 (Figures 3 and 4). Control mice showed 3.13 mm³ of BV, a TV of 73.34 mm³, a TbN of 2.52/mm, a TbTh of 0.14 mm, and a TbSp of 1.44 mm. In comparison, injured mice resulted in 3.19 mm³ of BV, a TV of 69.08, a TbN of 2.23/mm, a TbTh of 0.15 mm, and a TbSp of 1.37 mm. No significance was detected between the control and injured mice.

Since the radiographs indicated a possible BMP-2 batch effect, analysis was also performed with batch as a variable. Batch 1 resulted in a BV of 3.39 mm³, TV of 100.52 mm³, TbN of 0.84/mm, TbTH of 0.14 mm, and TbSp of 1.87 mm. Compared to Batch 2, which resulted in a BV of 2.71 mm³, TV of 12.58 mm³, TbN of 5.45/mm, TbTh of 0.16 mm, and TbSp of 0.45 mm. Comparison of differences between batches of BMP-2 showed a significance in BV ($p < 0.05$), TV ($p < 0.01$), TbN ($p < 0.01$), TbTh ($p < 0.05$), and TbSp ($p < 0.01$).

Three-dimensional (3D) renderings of the femur and ectopic bone were created to demonstrate the position of ectopic bone along the periosteal surface of the femur (Figure 5). The samples from the first batch demonstrated ectopic osteogenesis at the cortical bone/implant interface and along the periphery of the implant. Conversely, the samples that received the second batch of BMP-2 had ectopic bone localized along the length of the cortical bone extending beyond the limits of batch 1. This can be seen on 3D renderings and individual slices of the μ CT scan (Figure 6). This indicates that there was a batch effect due to the BMP-

2; however, the batch effect was restricted to a limited number of POD 16 and not included for further analysis.

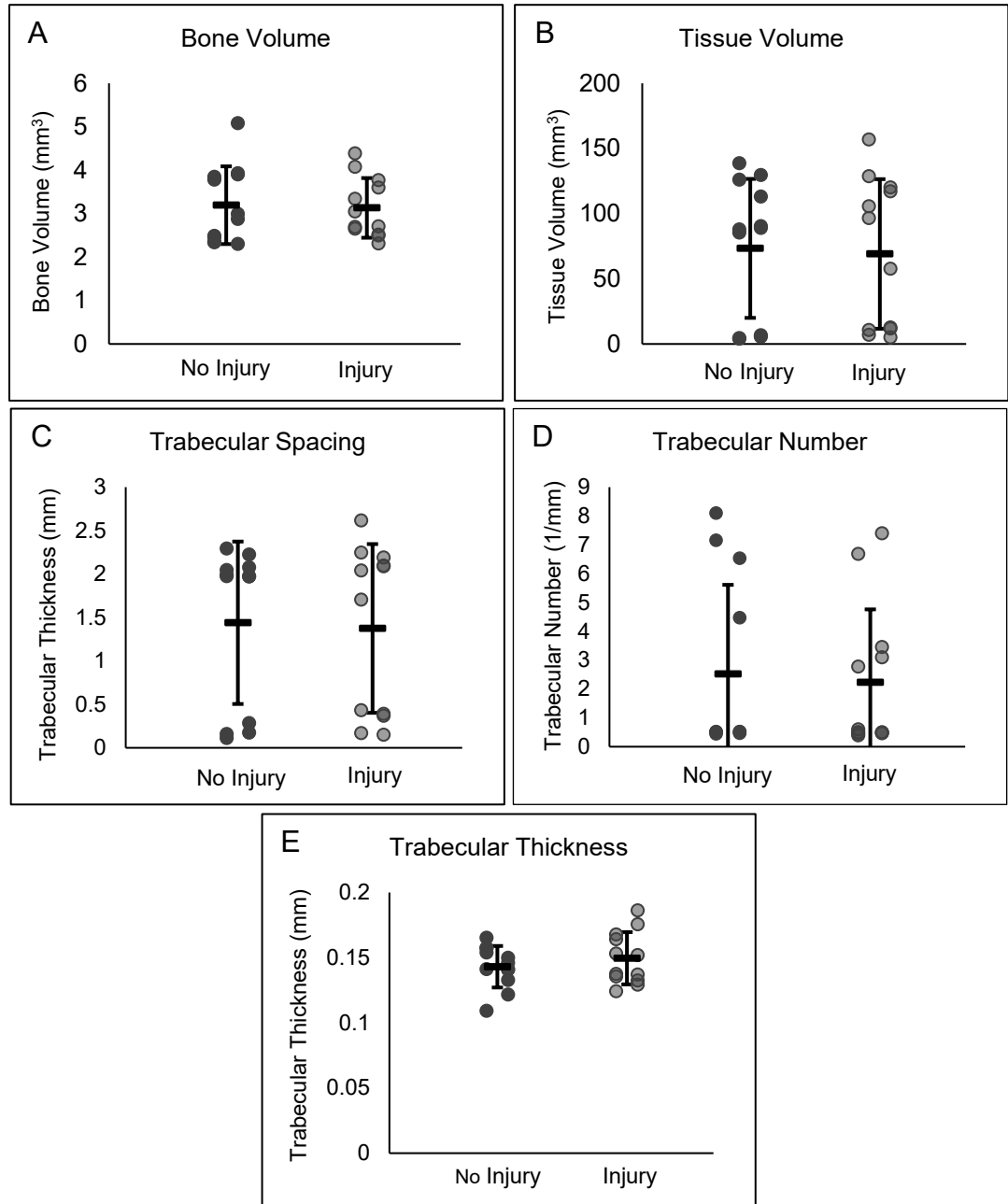


Figure 3: Effect of Injury on Ectopic Bone. Samples were implanted with a gelatin sponge containing 0.3 μg of BMP-2 with or without injury and harvested on POD 16. Samples here are not separated by batch. Sample size for each group is $n=12$. A-E) Scatter plots comparing bone volume, tissue volume, trabecular number, trabecular thickness and trabecular spacing, respectively, between injury groups.

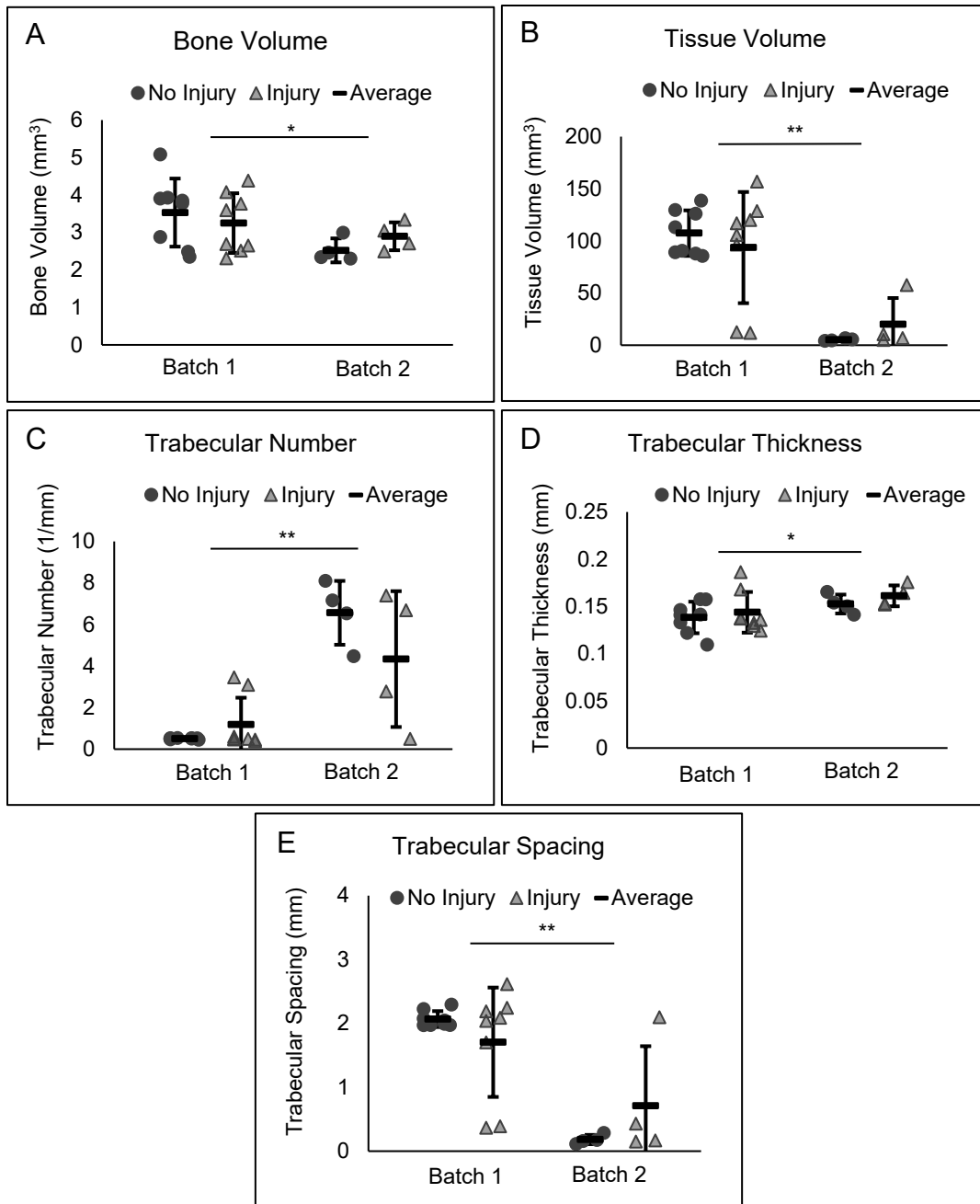


Figure 4: Effect of BMP-2 Batch on Ectopic Bone. Samples were implanted with a gelatin sponge containing 0.3 μg of BMP-2 and harvested on POD 16. Samples from Batch 1 receive BMP-2 from the first batch and Batch 2 received BMP-2 from a second batch. Samples sizes were as follows: Batch 1 $n=16$ and Batch 2 $n=8$. A-E) Scatter plots comparing bone volume, tissue volume, trabecular number, trabecular thickness and trabecular spacing, respectively, between BMP-2 batch groups. * represented a significance of $p < 0.05$, and ** represented a significance of $p < 0.01$.

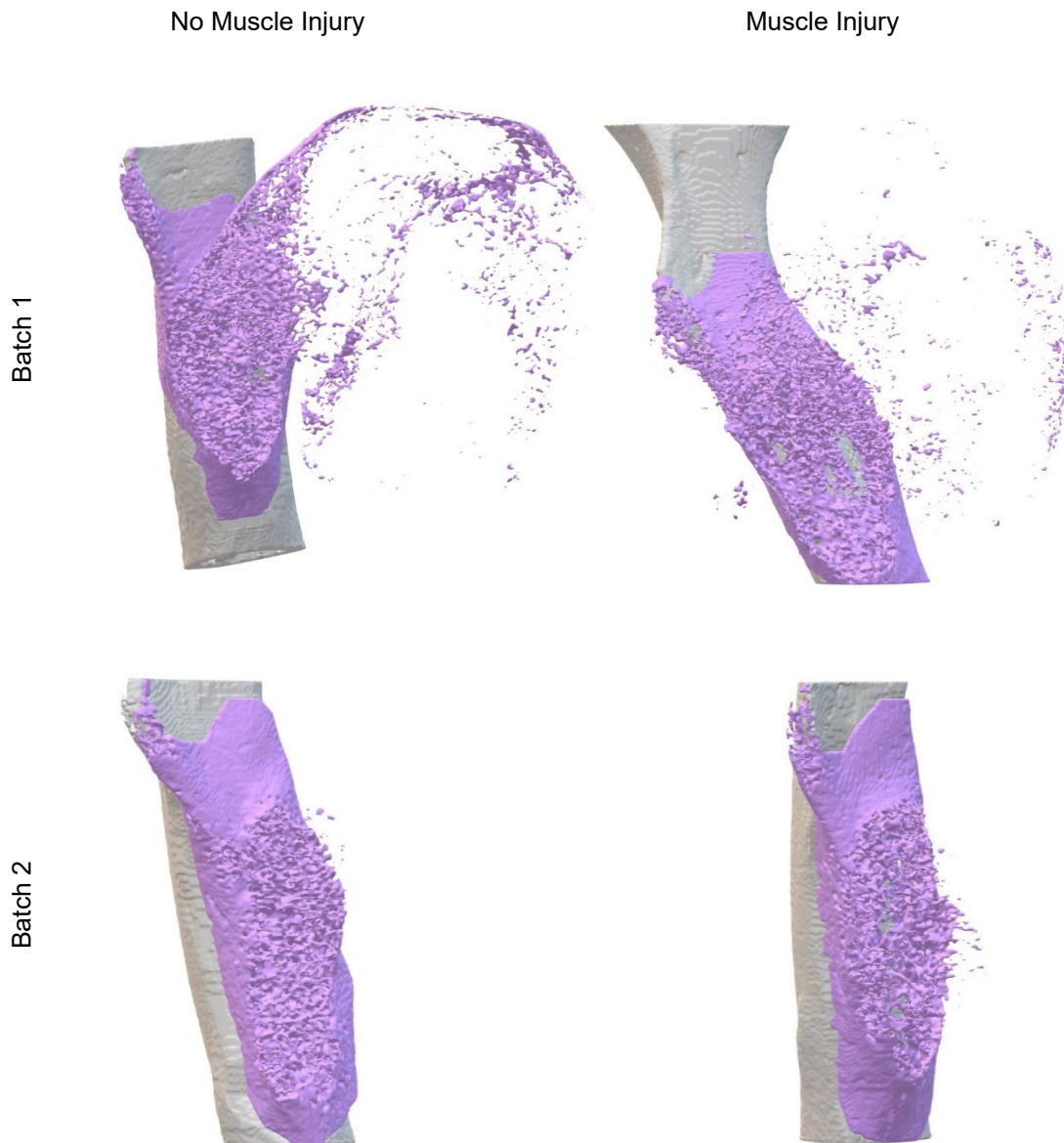


Figure 5: 3D Renderings Demonstrating Effect of BMP-2 Batch on Tissue Mineralization. Above are 3-dimensional renderings of periosteal ectopic bone along the femur. Note the proximal and distal ends of the femurs were not imaged as the ectopic bone did not extend beyond what is shown in the image. All the above samples were implanted with 0.3 μg of BMP-2 loaded into Surgifoam® Absorbable Gelatin Sponge with or without injury and harvested at POD 16. Purple represents ectopic bone. Left panel presents samples which did not receive muscle trauma, while the right panel shows samples in which trauma was induced following implantation. The top panel shows samples which received BMP-2 from the initial batch, and the bottom panel shows samples that were implanted with a second batch of BMP-2.

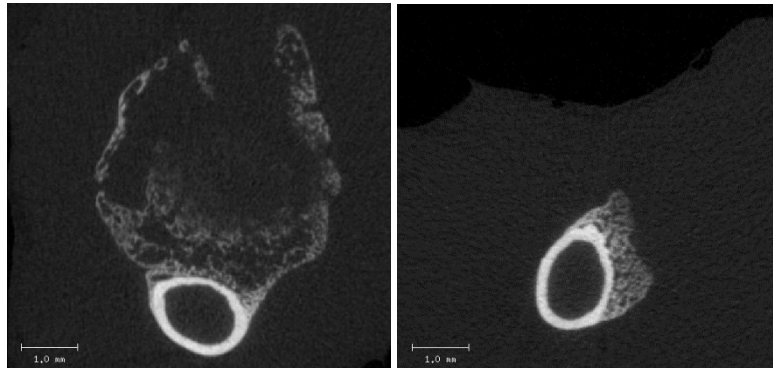


Figure 6: Position of Ectopic Bone Along the Femur. Above are cuts from the middle of the stack of μ CT images taken of the femur and ectopic bone. The right panel contains a cut from a sample from batch 1 of BMP-2, while the left panel contains a cut from a sample that received the BMP-2 from the second batch.

Comparing Gene Expression within the Implant During Ectopic Ossification

In determining the effect of muscle trauma on ectopic ossification, quantitative polymerase chain reaction (qPCR) was used to measure the gene expression within the developing ectopic bone tissue from both control and injured mice at POD 2, 8, and 16. All samples used were from the second batch of BMP-2. The relative expression of genes specific to endochondral ossification was quantified. Expression fold change was calculated relative to naïve mice, which did not undergo implantation surgery or injury, and was normalized to the 18s ribosomal RNA housekeeping gene.

Stem Cell Marker Expression

Paired related homeobox 1 (*Prx1*), sex determining region Y (*SRY*)-box 2 (*Sox2*), paired box 7 (*Pax7*), and alpha-smooth muscle actin (α -SMA) are stem cell markers that appear early during development of the musculoskeletal

system. *Prx1* is an early marker of skeletogenesis appearing during embryonic development at the limb buds and is required for endochondral ossification (Kawanami et al., 2009; E. R. Moore et al., 2019). *Sox2* is also expressed early in embryonic development. It is responsible for the maintenance, pluripotency, and self-renew of embryonic stem cells. It is also expressed in adult stem cells and maintains these populations (Feng & Wen, 2015) while also being upregulated during fracture repair (Bais et al., 2009). *Pax7* has been well established to be a marker for satellite cells, a skeletal muscle stem cell, and previous research has shown that these cells can transdifferentiate into a chondrogenic lineage and participate in endochondral ossification (Abou-Khalil et al., 2015). Lastly, α -SMA is predominantly known as a marker for perivascular stem cell populations, but has also been shown to be expressed by satellite cells, which demonstrate regenerative capabilities during angiogenesis; however, more recent research has shown that this population of cells can transdifferentiate into osteogenic cells (Matthews et al., 2016; Wanjare et al., 2013).

Prx1, *Pax7*, *Sox2*, and α -SMA expression were observed at POD 2, 8, and 16 in both control and injured animals. *Prx1* expression significantly increased at POD 8 ($p < 0.01$) and 16 ($p < 0.05$) compared to POD 2 for both control and injured groups. No significant difference was observed between POD 8 and 16. *Pax7* did not show significant temporal changes; however, there was an increased expression compared to naïve femur tissue. Conversely, *Sox2* expression peaked early at POD 2 compared to POD 8 ($p < 0.05$) and 16 ($p <$

0.01). Lastly, α -SMA showed significantly higher expression peaking at POD 8 compared to both POD 2 ($p < 0.01$) and POD 16 ($p < 0.01$). A significant difference was also seen between POD 2 and POD 16 ($p < 0.05$) (Figure 7). No significant differences were observed between sex or injury groups.

Chondrogenesis Marker Expression

Sox9, *Acan*, and *Col10a1* were used to detect chondrogenesis.

Expression of chondrogenic markers was observed at POD 8 and 16. *Sox9* and *Acan* expression peaked in both control and injury groups at POD 8, while *Col10a1* expression was highest at POD 16 in both control and injured samples. No significant differences were observed between sex or injury groups (Figure 8).

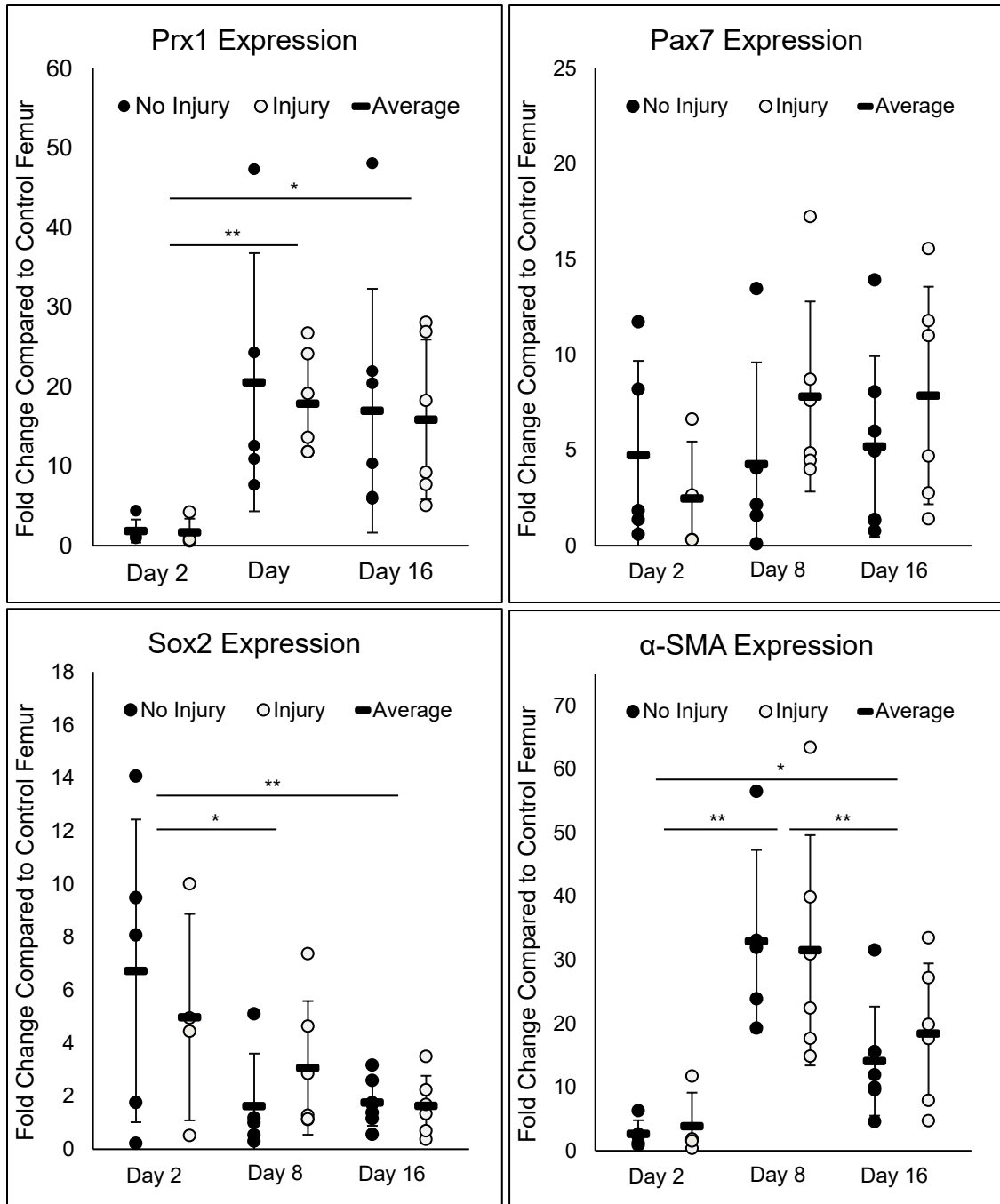


Figure 7: Comparison of Stem Cell Markers in Ectopic Bone Over Time. Above are scatter plots comparing the expression Prx1, Pax7, Sox2 and α-SMA at POD 2, 8, and 16. Samples sizes are as follows: POD 2 No Injury n = 5, POD 2 Injury n=4, POD 8 No Injury n = 5, POD 8 Injury n = 6, POD 16 No Injury n = 7, and POD 16 Injury n = 6. Significance is represented with * for a p < 0.05, and ** for a p < 0.01.

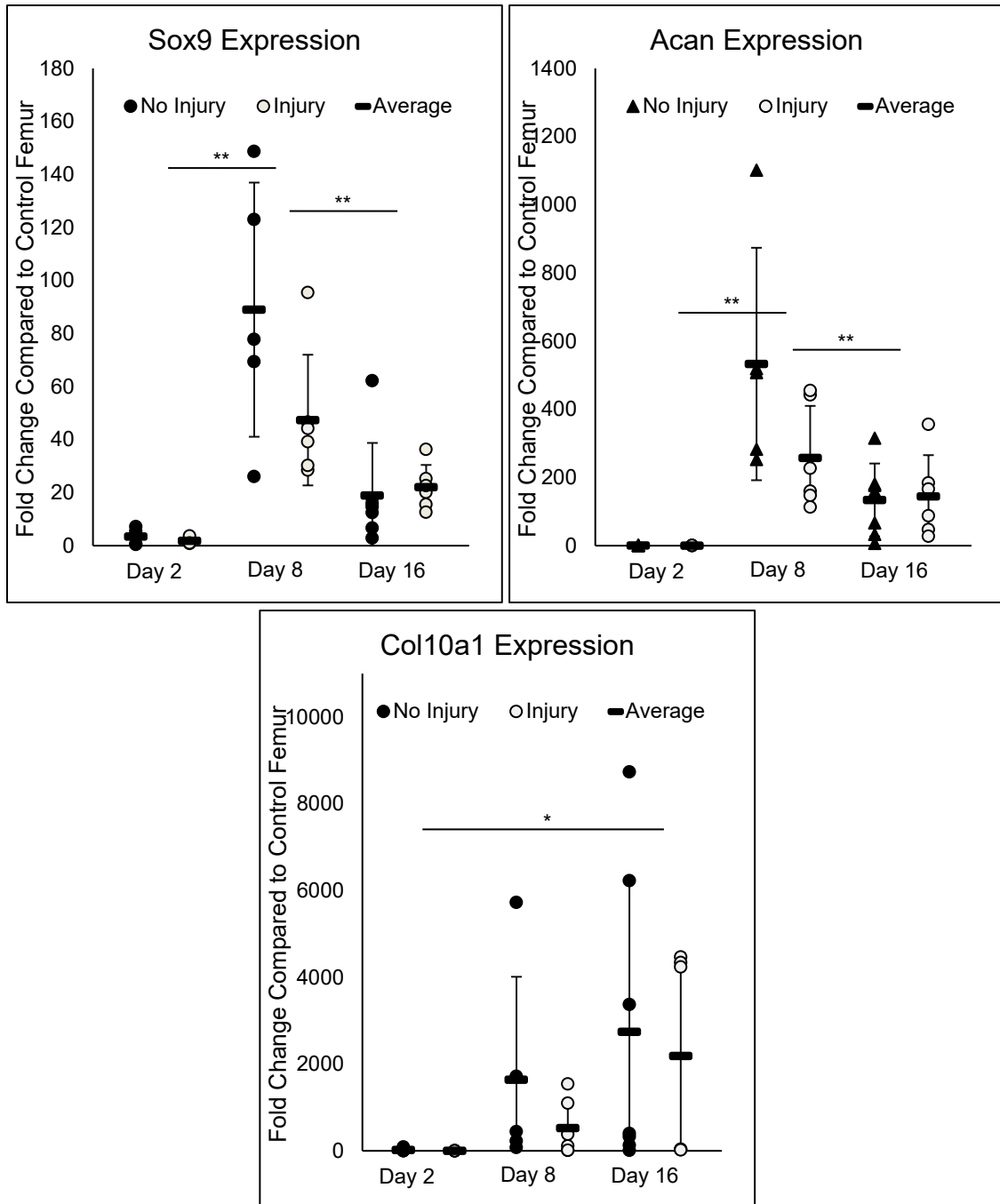


Figure 8: Comparison of Chondrogenic Markers in Ectopic Bone Over Time. Above are scatter plots comparing the expression Sox9, Acan and Col10a1 at POD 2, 8, and 16. Samples sizes are as follows: POD 2 No Injury n = 5 (Sox9 and Acan n = 4), POD 2 Injury n=4 (Sox9 and Acan n = 3), POD 8 No Injury n = 5, POD 8 Injury n = 6, POD 16 No Injury n = 7, and POD 16 Injury n = 6. Of note Sox9 and Acan both had Significance is represented with * for a $p < 0.05$, and ** for a $p < 0.01$.

Osteogenesis Marker Expression

Osteogenic gene expression was measured using *RUNX2*, *Sp7*, and *DMP-1*. For each osteogenic gene, expression peaked at POD 16. Significance was seen in the expression of *RUNX2* between POD 16 and both POD 2 ($p < 0.01$) and POD 8 ($p < 0.05$). Significance for *Sp7* was only observed between POD 16 and 2 ($p < 0.05$), while significance with *DMP-1* expression was only observed between POD 16 and 8 ($p < 0.05$) (Figure 9).

BMP Signaling Expression

Expression of genes involved in the BMP signaling cascade was measured using the markers *BMP-2*, *BMP-7*, *Id-1*, and myostatin (*MSTN*). Animals harvested at POD 16 expressed the highest amount of *BMP-2* and *BMP-7*. A significant difference with *BMP-2* expression was observed between POD 2 and 16 ($p < 0.01$). Additionally, *BMP-7* expression was significantly different between POD 16 and both POD 2 and 8 at a significance of $p < 0.05$. *Id-1* and *MSTN* showed no significant differences between harvest times (Figure 10).

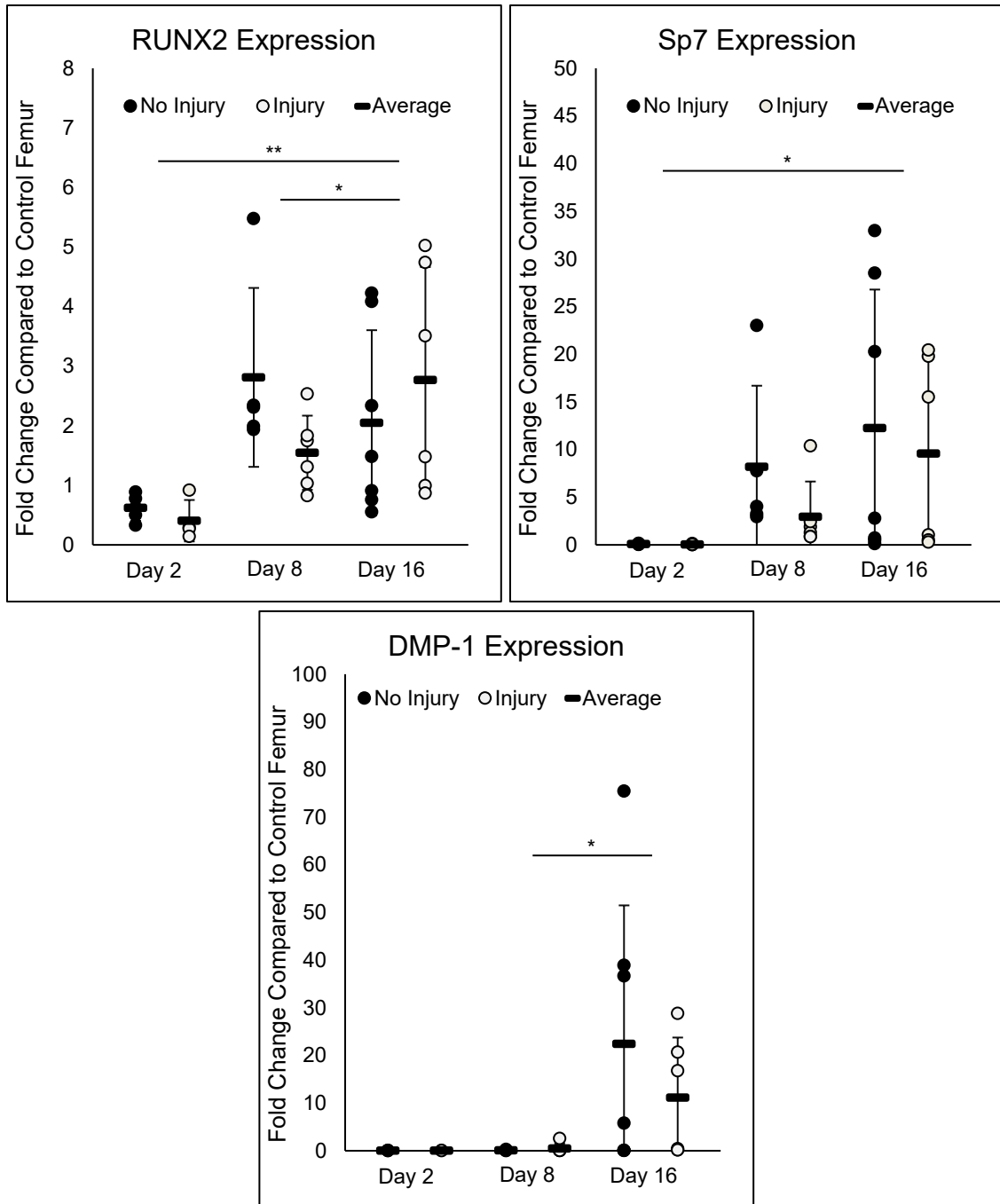


Figure 9: Comparison of Osteogenic Markers in Ectopic Bone Over Time. Above are scatter plots comparing the expression RUNX2, Sp7 and DMP-1 at POD 2, 8, and 16. Samples sizes are as follows: POD 2 No Injury n = 5 (DMP-1 n = 3), POD 2 Injury n=4 (DMP-1 n = 2), POD 8 No Injury n = 5, POD 8 Injury n = 6, POD 16 No Injury n = 7, and POD 16 Injury n = 6. Significance is represented with * for a p < 0.05, and ** for a p < 0.01.

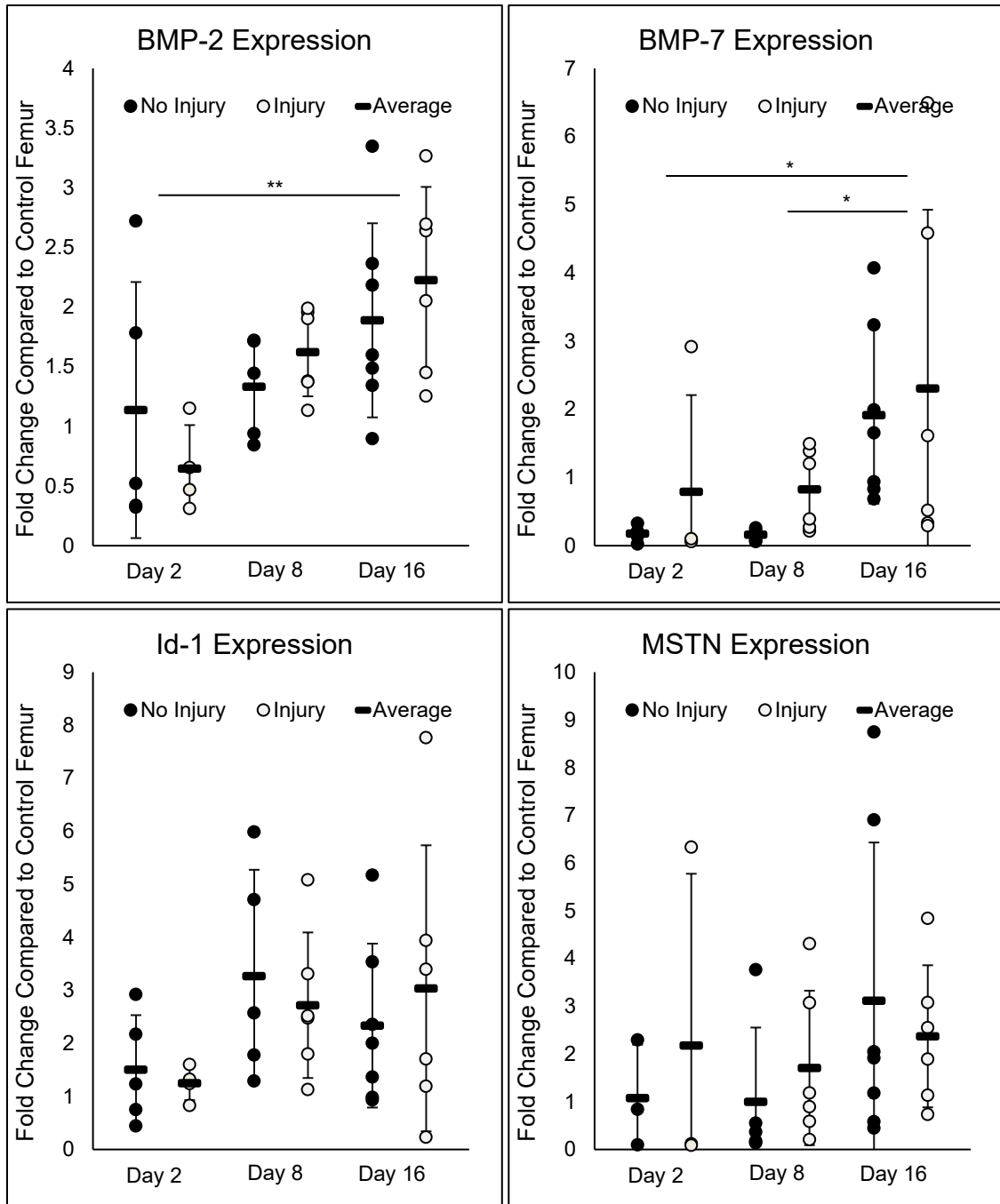


Figure 10: Comparison of BMP Signaling Markers in Ectopic Bone Over Time. Above are scatter plots comparing the expression BMP-2, BMP-7, Id-1 and MSTN at POD 2, 8, and 16. Samples sizes are as follows: POD 2 No Injury n = 5 (MSTN n = 3), POD 2 Injury n=4 (MSTN n = 3), POD 8 No Injury n = 5, POD 8 Injury n = 6, POD 16 No Injury n = 7, and POD 16 Injury n = 6. Significance is represented with * for a p < 0.5, and ** for a p < 0.01.

DISCUSSION

Effect of BMP-2 Batch on Ectopic Bone

Periosteal gelatin sponge implants loaded with BMP-2 induced endochondral heterotopic ossification in both injured and control mice. However, a batch effect was observed in our study, which interestingly resulted in the formation of ectopic bone of similar volume but differed in tissue volume and trabecular morphology. Bone tissue was distributed unevenly, with the first batch samples showing tissue at the cortical bone/implant interface and along the periphery of the implant. In contrast, the second batch was localized along the periosteal surface. These differences were observed on plain film radiographs, and 3D renderings of the samples of samples harvest POD 16 (Figures 4, 5, and 6). These findings suggest that there was a change between the batches of BMP-2 used in this study, likely a result of human error in handling or preparation.

Effects of Muscle Trauma Ectopic Bone Development

A comparison of ectopic bone volumes (BV), tissue volumes (TV), trabecular number (TbN), trabecular thickness (TbTh), and trabecular spacing (TbSp) showed no significant differences between injury cohorts. These findings are not consistent with published literature (Li et al., 2019) or previous findings in the lab, which showed muscle injury does enhance ectopic bone formation resulting in increased bone volume (W. T. Moore, 2019). An explanation of this

inconsistent observation could be that the dose of BMP-2 used in the study was enough to stimulate ectopic bone formation in both sample groups regardless of whether an injury or no injury was induced. Furthermore, a previous study showed that that gelatin sponge as opposed to a collagen gel and fibrin sealant produced hypertrophic bone, whereas the other models formed bone resemblant of the surrounding bone (Usas et al., 2009). This could offer another explanation on why this study showed nearly twice as much bone volume in both control and injured samples compared to samples in previous work in the lab (W. T. Moore, 2019). Future experiments using a 0.1 µg of BMP-2 could be performed to see if a lower dose of BMP-2 results in a difference between control and injured animals.

Variations in Gene Expression in Heterotopic Ossification Over Time

This study suggests that varying stem cell populations contribute to ectopic bone formation; however, the temporal progression may be unique to the differing stem cell populations. *Sox2* was the only gene investigated that showed peak expression as POD 2, suggesting an early presence of adult stem cells in the implant. The stark drop in expression of *Sox2* at POD 8 and 16 suggests the loss of pluripotency and progression of cell differentiation (Zhang & Cui, 2014). Both *Prx1* and *α-SMA* showed increased expression at POD 8 and was maintained through POD16. It was not surprising that both populations of cells contribute to postnatal bone formation based on previous studies (Bennie, 2017;

Matthews et al., 2016). However, the later peak and maintenance was interesting and may suggest that these cell populations expand during endochondral ossification or that these transcription factors are regulating cell differentiation and function, as suggested by Esposito et al. (2020). Although *Pax7* expression did not change across time, there was increased expression compared to the naïve femur tissue. Since *Pax7* is a muscle satellite stem cell marker, this indicates that there may be a recruitment of cells from the surrounding muscle.

In general, the expression of chondrogenic and osteogenic genes is consistent with the stages of endochondral ossification. Early chondrogenic genes, *Sox9* and *Acan*, peak expression at POD 8, while late-stage chondrogenic gene *Col10a1* and osteogenic genes peaked at POD 16. These results are consistent with previous findings that demonstrated peak chondrogenic gene expression at POD 8, while osteoblast-specific genes peaked later at POD 16 animals (B. Bragdon et al., 2017). Conversely, this study did show *Col10a1* peaking at POD 16, which suggests that there may be a delay in osteogenesis. Similar to the osteogenic gene expression BMP-2 and BMP-7 signaling was expressed at higher POD 16 compared to POD 2 and 8. However, expression of *Id-1* was comparable at all time points, despite this gene being downstream of BMP-2 and BMP-7 in the BMP signaling cascade. This observation could be explained by the supplementation of BMP-2 during surgical implantation. As observed in previous research (Katagiri et al., 2002), BMP-2

stimulates the expression of Id-1, which would explain the early expression of Id-1. Similarly, *MSTN* expression was constant at all three time points, consistent with data from previous research in the lab (Murphy, 2020).

Conclusion and Limitations

The impact of muscle injury on the development of ectopic bone is difficult to assess with this study's results. However, significant gene expression changes were observed that reaffirmed previous findings regarding the specific pattern correlating with the progression through endochondral ossification, particularly chondrogenesis peaking at POD 8 and osteogenesis present in POD 16 animals. However, small differences between injury groups are hard to distinguish due to the small sample size in each cohort and high variance within groups. Further studies on the expression of endochondral ossification genes in developing ectopic bone would further our general understanding and lead to more significant findings within groups. Furthermore, this study did suggest the possibility of some delay in osteogenesis in the POD 16 samples, which could indicate the need to study the gene expression of implants at later time points, like POD 21 or 31.

Micro-computed tomography data identified a batch effect within the study. The appearance of a batch effect introduced a new confounding variable with stark differences between both batches. These differences limited the ability to compare injured and uninjured samples in the μ CT analysis of the ectopic bone

due to the small sample size for batch 2. Though some trend was noticeable when removing the initial batch samples from the analysis, this population was too small to provide any significant comparison. Further studies using the same animal model would increase sampling and provide a better representation of the effects of muscle trauma on bone formation.

REFERENCES

- Abou-Khalil, R., Yang, F., Lieu, S., Julien, A., Perry, J., Pereira, C., Relaix, F., Miclau, T., Marcucio, R., & Colnot, C. (2015). Role of Muscle Stem Cells During Skeletal Regeneration. *STEM CELLS*, 33(5), 1501–1511. <https://doi.org/10.1002/stem.1945>
- Akiyama, H., Chaboissier, M.-C., Martin, J. F., Schedl, A., & de Crombrughe, B. (2002). The transcription factor Sox9 has essential roles in successive steps of the chondrocyte differentiation pathway and is required for expression of Sox5 and Sox6. *Genes & Development*, 16(21), 2813–2828. <https://doi.org/10.1101/gad.1017802>
- Akiyama, H., & Lefebvre, V. (2011). Unraveling the transcriptional regulatory machinery in chondrogenesis. *Journal of Bone and Mineral Metabolism*, 29(4), 390–395. <https://doi.org/10.1007/s00774-011-0273-9>
- Allas, L., Boumédiène, K., & Baugé, C. (2019). Epigenetic dynamic during endochondral ossification and articular cartilage development. *Bone*, 120, 523–532. <https://doi.org/10.1016/j.bone.2018.10.004>
- Arnold, L., Henry, A., Poron, F., Baba-Amer, Y., van Rooijen, N., Plonquet, A., Gherardi, R. K., & Chazaud, B. (2007). Inflammatory monocytes recruited after skeletal muscle injury switch into antiinflammatory macrophages to support myogenesis. *The Journal of Experimental Medicine*, 204(5), 1057–1069. <https://doi.org/10.1084/jem.20070075>
- Bais, M., McLean, J., Sebastiani, P., Young, M., Wigner, N., Smith, T., Kotton, D. N., Einhorn, T. A., & Gerstenfeld, L. C. (2009). Transcriptional Analysis of Fracture Healing and the Induction of Embryonic Stem Cell-Related Genes. *PLOS ONE*, 4(5), e5393. <https://doi.org/10.1371/journal.pone.0005393>
- Barfield, W. R., Holmes, R. E., & Hartsock, L. A. (2017). Heterotopic Ossification in Trauma. *The Orthopedic Clinics of North America*, 48(1), 35–46. <https://doi.org/10.1016/j.ocl.2016.08.009>
- Bennie, A. (2017). *Lineage Tracing of Skeletal Progenitor Cells during Postnatal Bone Formation* [M.S., Boston University]. <http://search.proquest.com/pqdtglobal/docview/1929900121/abstract/94DA1BF1590840DDPQ/8>

- Berendsen, A. D., & Olsen, B. R. (2015). Bone development. *Bone*, *80*, 14–18. <https://doi.org/10.1016/j.bone.2015.04.035>
- Bi, W., Deng, J. M., Zhang, Z., Behringer, R. R., & de Crombrughe, B. (1999). Sox9 is required for cartilage formation. *Nature Genetics*, *22*(1), 85–89. <https://doi.org/10.1038/8792>
- Bi, W., Huang, W., Whitworth, D. J., Deng, J. M., Zhang, Z., Behringer, R. R., & de Crombrughe, B. (2001). Haploinsufficiency of Sox9 results in defective cartilage primordia and premature skeletal mineralization. *Proceedings of the National Academy of Sciences of the United States of America*, *98*(12), 6698–6703. <https://doi.org/10.1073/pnas.111092198>
- Bragdon, B. C., & Bahney, C. S. (2018). Origin of Reparative Stem Cells in Fracture Healing. *Current Osteoporosis Reports*, *16*(4), 490–503. <https://doi.org/10.1007/s11914-018-0458-4>
- Bragdon, B., Lam, S., Aly, S., Femia, A., Clark, A., Hussein, A., Morgan, E. F., & Gerstenfeld, L. C. (2017). Earliest phases of chondrogenesis are dependent upon angiogenesis during ectopic bone formation in mice. *Bone*, *101*, 49–61. <https://doi.org/10.1016/j.bone.2017.04.002>
- Bragdon, B., Moseychuk, O., Saldanha, S., King, D., Julian, J., & Nohe, A. (2011). Bone Morphogenetic Proteins: A critical review. *Cellular Signalling*, *23*(4), 609–620. <https://doi.org/10.1016/j.cellsig.2010.10.003>
- Breeland, G., Sinkler, M. A., & Menezes, R. G. (2020). Embryology, Bone Ossification. In *StatPearls*. StatPearls Publishing. <http://www.ncbi.nlm.nih.gov/books/NBK539718/>
- Buza, J. A., & Einhorn, T. (2016). Bone healing in 2016. *Clinical Cases in Mineral and Bone Metabolism*, *13*(2), 101–105. <https://doi.org/10.11138/ccmbm/2016.13.2.101>
- Cappato, S., Gamberale, R., Bocciardi, R., & Brunelli, S. (2020). Genetic and Acquired Heterotopic Ossification: A Translational Tale of Mice and Men. *Biomedicines*, *8*(12). <https://doi.org/10.3390/biomedicines8120611>
- Chan, J. K.-K., Harry, L., Williams, G., & Nanchahal, J. (2012). Soft Tissue Reconstruction of Open Fractures of the Lower Limb: Muscle versus fasciocutaneous flaps. *Plastic and Reconstructive Surgery*, *130*(2), 284e–295e. <https://doi.org/10.1097/PRS.0b013e3182589e63>

- Chen, B., & Shan, T. (2019). The role of satellite and other functional cell types in muscle repair and regeneration. *Journal of Muscle Research and Cell Motility*, 40(1), 1–8. <https://doi.org/10.1007/s10974-019-09511-3>
- Coates, B. A., McKenzie, J. A., Buettmann, E. G., Liu, X., Gontarz, P. M., Zhang, B., & Silva, M. J. (2019). Transcriptional Profiling of Intramembranous and Endochondral Ossification after Fracture in Mice. *Bone*, 127, 577–591. <https://doi.org/10.1016/j.bone.2019.07.022>
- de Crombrughe, B., Lefebvre, V., Behringer, R. R., Bi, W., Murakami, S., & Huang, W. (2000). Transcriptional mechanisms of chondrocyte differentiation. *Matrix Biology*, 19(5), 389–394. [https://doi.org/10.1016/S0945-053X\(00\)00094-9](https://doi.org/10.1016/S0945-053X(00)00094-9)
- Einhorn, T. A., & Gerstenfeld, L. C. (2015). Fracture healing: Mechanisms and interventions. *Nature Reviews. Rheumatology*, 11(1), 45–54. <https://doi.org/10.1038/nrrheum.2014.164>
- Eisenstein, N., Stapley, S., & Grover, L. (2018). Post-Traumatic Heterotopic Ossification: An Old Problem in Need of New Solutions. *Journal of Orthopaedic Research: Official Publication of the Orthopaedic Research Society*, 36(4), 1061–1068. <https://doi.org/10.1002/jor.23808>
- Ekegren, C. L., Edwards, E. R., de Steiger, R., & Gabbe, B. J. (2018). Incidence, Costs and Predictors of Non-Union, Delayed Union and Mal-Union Following Long Bone Fracture. *International Journal of Environmental Research and Public Health*, 15(12). <https://doi.org/10.3390/ijerph15122845>
- Esposito, A., Wang, L., Li, T., Miranda, M., & Spagnoli, A. (2020). Role of Prx1-expressing skeletal cells and Prx1-expression in fracture repair. *Bone*, 139, 115521. <https://doi.org/10.1016/j.bone.2020.115521>
- Feng, R., & Wen, J. (2015). Overview of the roles of Sox2 in stem cell and development. *Biological Chemistry*, 396(8), 883–891. <https://doi.org/10.1515/hsz-2014-0317>
- Frontera, W. R., & Ochala, J. (2015). Skeletal Muscle: A Brief Review of Structure and Function. *Calcified Tissue International*, 96(3), 183–195. <https://doi.org/10.1007/s00223-014-9915-y>
- Grode, J., Hardin, K., & Oberfeld, B. (2017). *Examining Muscle-Bone Crosstalk: Design of Muscle Trauma Model for Study of Stem Cell Recruitment in Injury Repair*.

- Hallett, S. A., Ono, W., & Ono, N. (2019). Growth Plate Chondrocytes: Skeletal Development, Growth and Beyond. *International Journal of Molecular Sciences*, 20(23). <https://doi.org/10.3390/ijms20236009>
- Han, Y., & Lefebvre, V. (2008). L-Sox5 and Sox6 Drive Expression of the Aggrecan Gene in Cartilage by Securing Binding of Sox9 to a Far-Upstream Enhancer. *Molecular and Cellular Biology*, 28(16), 4999–5013. <https://doi.org/10.1128/MCB.00695-08>
- Harry, L. E., Sandison, A., Paleolog, E. M., Hansen, U., Pearse, M. F., & Nanchahal, J. (2008). Comparison of the healing of open tibial fractures covered with either muscle or fasciocutaneous tissue in a murine model. *Journal of Orthopaedic Research*, 26(9), 1238–1244. <https://doi.org/10.1002/jor.20649>
- Hata, K., Takahata, Y., Murakami, T., & Nishimura, R. (2017). Transcriptional Network Controlling Endochondral Ossification. *Journal of Bone Metabolism*, 24(2), 75–82. <https://doi.org/10.11005/jbm.2017.24.2.75>
- Hattori, T., Müller, C., Gebhard, S., Bauer, E., Pausch, F., Schlund, B., Bösl, M. R., Hess, A., Surmann-Schmitt, C., Mark, H. von der, Crombrugge, B. de, & Mark, K. von der. (2010). SOX9 is a major negative regulator of cartilage vascularization, bone marrow formation and endochondral ossification. *Development*, 137(6), 901–911. <https://doi.org/10.1242/dev.045203>
- Kan, C., Chen, L., Hu, Y., Ding, N., Lu, H., Li, Y., Kessler, J. A., & Kan, L. (2018). Conserved signaling pathways underlying heterotopic ossification. *Bone*, 109, 43–48. <https://doi.org/10.1016/j.bone.2017.04.014>
- Kan, L., & Kessler, J. A. (2011). Animal Models of Typical Heterotopic Ossification. *Journal of Biomedicine and Biotechnology*, 2011. <https://doi.org/10.1155/2011/309287>
- Kaplan, F. S., Pignolo, R. J., & Shore, E. M. (2013). From mysteries to medicines: Drug development for fibrodysplasia ossificans progressive. *Expert Opinion on Orphan Drugs*, 1(8), 637–649. <https://doi.org/10.1517/21678707.2013.825208>
- Katagiri, T., Imada, M., Yanai, T., Suda, T., Takahashi, N., & Kamijo, R. (2002). Identification of a BMP-responsive element in Id1, the gene for inhibition of myogenesis. *Genes to Cells*, 7(9), 949–960. <https://doi.org/10.1046/j.1365-2443.2002.00573.x>

- Katagiri, T., Osawa, K., Tsukamoto, S., Fujimoto, M., Miyamoto, A., & Mizuta, T. (2015). Bone morphogenetic protein-induced heterotopic bone formation: What have we learned from the history of a half century? *Japanese Dental Science Review*, 51(2), 42–50. <https://doi.org/10.1016/j.jdsr.2014.09.004>
- Kawanami, A., Matsushita, T., Chan, Y. Y., & Murakami, S. (2009). Mice expressing GFP and CreER in osteochondro progenitor cells in the periosteum. *Biochemical and Biophysical Research Communications*, 386(3), 477–482. <https://doi.org/10.1016/j.bbrc.2009.06.059>
- Komori, T., Yagi, H., Nomura, S., Yamaguchi, A., Sasaki, K., Deguchi, K., Shimizu, Y., Bronson, R. T., Gao, Y.-H., Inada, M., Sato, M., Okamoto, R., Kitamura, Y., Yoshiki, S., & Kishimoto, T. (1997). Targeted Disruption of Cbfa1 Results in a Complete Lack of Bone Formation owing to Maturational Arrest of Osteoblasts. *Cell*, 89(5), 755–764. [https://doi.org/10.1016/S0092-8674\(00\)80258-5](https://doi.org/10.1016/S0092-8674(00)80258-5)
- Li, L., Jiang, Y., Lin, H., Shen, H., Sohn, J., Alexander, P. G., & Tuan, R. S. (2019). Muscle injury promotes heterotopic ossification by stimulating local bone morphogenetic protein-7 production. *Journal of Orthopaedic Translation*, 18, 142–153. <https://doi.org/10.1016/j.jot.2019.06.001>
- Liu, X., Kang, H., Shahnazari, M., Kim, H., Wang, L., Larm, O., Adolfsson, L., Nissenson, R., & Halloran, B. (2014). A novel mouse model of trauma induced heterotopic ossification. *Journal of Orthopaedic Research*, 32(2), 183–188. <https://doi.org/10.1002/jor.22500>
- Long, F., & Ornitz, D. M. (2013). Development of the Endochondral Skeleton. *Cold Spring Harbor Perspectives in Biology*, 5(1). <https://doi.org/10.1101/cshperspect.a008334>
- Matsushita, Y., Ono, W., & Ono, N. (2020). Skeletal Stem Cells for Bone Development and Repair: Diversity Matters. *Current Osteoporosis Reports*, 18(3), 189–198. <https://doi.org/10.1007/s11914-020-00572-9>
- Matthews, B. G., Torreggiani, E., Roeder, E., Matic, I., Grcevic, D., & Kalajzic, I. (2016). Osteogenic potential of alpha smooth muscle actin expressing muscle resident progenitor cells. *Bone*, 84, 69–77. <https://doi.org/10.1016/j.bone.2015.12.010>
- Meyers, C., Lisiecki, J., Miller, S., Levin, A., Fayad, L., Ding, C., Sono, T., McCarthy, E., Levi, B., & James, A. W. (2019). Heterotopic Ossification: A

Comprehensive Review. *JBMR Plus*, 3(4), e10172.
<https://doi.org/10.1002/jbm4.10172>

Moore, E. R., Chen, J. C., & Jacobs, C. R. (2019). Prx1-Expressing Progenitor Primary Cilia Mediate Bone Formation in response to Mechanical Loading in Mice. *Stem Cells International*, 2019, e3094154.
<https://doi.org/10.1155/2019/3094154>

Moore, W. T. (2019). *Impact of Muscle Trauma on Stem Cell Recruitment During Post-Natal Ectopic Bone Formation* [M.S., Boston University].
<http://search.proquest.com/pqdtglobal/docview/2275993314/abstract/249A8D05954F4C6EPQ/13>

Mukund, K., & Subramaniam, S. (2020). Skeletal muscle: A review of molecular structure and function, in health and disease. *Wiley Interdisciplinary Reviews. Systems Biology and Medicine*, 12(1).
<https://doi.org/10.1002/wsbm.1462>

Murphy, P. G. (2020). *Identifying the Role of Muscle Trauma on Heterotrophic Ossification* [M.S., Boston University].
<http://search.proquest.com/pqdtglobal/docview/2437202129/abstract/249A8D05954F4C6EPQ/3>

Nakashima, K., Zhou, X., Kunkel, G., Zhang, Z., Deng, J. M., Behringer, R. R., & Crombrughe, B. de. (2002). The Novel Zinc Finger-Containing Transcription Factor Osterix Is Required for Osteoblast Differentiation and Bone Formation. *Cell*, 108(1), 17–29. [https://doi.org/10.1016/S0092-8674\(01\)00622-5](https://doi.org/10.1016/S0092-8674(01)00622-5)

Ohba, S. (2020). Hedgehog Signaling in Skeletal Development: Roles of Indian Hedgehog and the Mode of Its Action. *International Journal of Molecular Sciences*, 21(18). <https://doi.org/10.3390/ijms21186665>

Pulik, Ł., Mierzejewski, B., Ciemerych, M. A., Brzóška, E., & Łęgosz, P. (2020). The Survey of Cells Responsible for Heterotopic Ossification Development in Skeletal Muscles-Human and Mouse Models. *Cells*, 9(6).
<https://doi.org/10.3390/cells9061324>

Richards, R., McKee, M., Paitich, C., Anderson, G., & Bertoia, J. (1991). A comparison of the effects of skin coverage and muscle flap coverage on the early strength of union at the site of osteotomy after devascularization of a segment of canine tibia. *The Journal of Bone & Joint Surgery*, 73(9), 1323–1330.

- Schmidt, M., Schüler, S. C., Hüttner, S. S., von Eyss, B., & von Maltzahn, J. (2019). Adult stem cells at work: Regenerating skeletal muscle. *Cellular and Molecular Life Sciences*, 76(13), 2559–2570. <https://doi.org/10.1007/s00018-019-03093-6>
- Shore, E. M., Xu, M., Feldman, G. J., Fenstermacher, D. A., Cho, T.-J., Choi, I. H., Connor, J. M., Delai, P., Glaser, D. L., LeMerrer, M., Morhart, R., Rogers, J. G., Smith, R., Triffitt, J. T., Urtizberea, J. A., Zasloff, M., Brown, M. A., & Kaplan, F. S. (2006). A recurrent mutation in the BMP type I receptor ACVR1 causes inherited and sporadic fibrodysplasia ossificans progressiva. *Nature Genetics*, 38(5), 525–527. <https://doi.org/10.1038/ng1783>
- St-Jacques, B., Hammerschmidt, M., & McMahon, A. P. (1999). Indian hedgehog signaling regulates proliferation and differentiation of chondrocytes and is essential for bone formation. *Genes & Development*, 13(16), 2072–2086.
- Usas, A., Ho, A. M., Cooper, G. M., Olshanski, A., Peng, H., & Huard, J. (2009). Bone Regeneration Mediated by BMP4-Expressing Muscle-Derived Stem Cells Is Affected by Delivery System. *Tissue Engineering. Part A*, 15(2), 285–293. <https://doi.org/10.1089/ten.tea.2008.0130>
- Vortkamp, A., Pathi, S., Peretti, G. M., Caruso, E. M., Zaleske, D. J., & Tabin, C. J. (1998). Recapitulation of signals regulating embryonic bone formation during postnatal growth and in fracture repair. *Mechanisms of Development*, 71(1), 65–76. [https://doi.org/10.1016/S0925-4773\(97\)00203-7](https://doi.org/10.1016/S0925-4773(97)00203-7)
- Wanjare, M., Kusuma, S., & Gerecht, S. (2013). Perivascular cells in blood vessel regeneration. *Biotechnology Journal*, 8(4), 434–447. <https://doi.org/10.1002/biot.201200199>
- Yin, H., Price, F., & Rudnicki, M. A. (2013). Satellite Cells and the Muscle Stem Cell Niche. *Physiological Reviews*, 93(1), 23–67. <https://doi.org/10.1152/physrev.00043.2011>
- Zhang, S., & Cui, W. (2014). Sox2, a key factor in the regulation of pluripotency and neural differentiation. *World Journal of Stem Cells*, 6(3), 305–311. <https://doi.org/10.4252/wjsc.v6.i3.305>

CURRICULUM VITAE

